IN-29
046915

Use of Microgravity to Control the Microstructure of Eutectics

NASA Grant NAG8-1266

Progress report: 1 March 1998 to 28 February 1999

Professors William R. Wilcox and Liya L. Regel
International Center for Gravity Materials Science and Applications
Clarkson University, Potsdam NY 13699-5814
phone: 1-315-268-7672
fax: 1-315-268-3833
email: wilcox@clarkson.edu and regel@clarkson.edu

ABSTRACT

This grant began in June of 1996. Its long term goal is to be able to control the microstructure of directionally solidified eutectic alloys, through an improved understanding of the influence of convection. The primary objective of the projects in the present grant is to test hypotheses for the reported influence of microgravity on the microstructure of eutectics.

The prior experimental results on the influence of microgravity on the microstructure of eutectics have been contradictory. With lamellar eutectics, microgravity had a negligible effect on the microstructure. Microgravity experiments with fibrous eutectics sometimes showed a finer microstructure and sometimes a coarser microstructure. Most research has been done on the MnBi/Bi rod-like eutectic. Larson and Pirich obtained a two-fold finer microstructure both from microgravity and by use of a magnetic field to quench buoyancy-driven convection. Smith, on the other hand, observed no change in microgravity.

Prior theoretical work at Clarkson University showed that buoyancy-driven convection in the vertical Bridgman configuration is not vigorous enough to alter the concentration field in front of a growing eutectic sufficiently to cause a measurable change in microstructure. We assumed that the bulk melt was at the eutectic composition and that freezing occurred at the extremum, i.e. with minimum total undercooling at the freezing interface.

There have been four hypotheses attempting to explain the observed changes in microstructure of fibrous eutectics caused by convection:

1. A fluctuating freezing rate, combined with unequal kinetics for fiber termination and branching.
2. Off-eutectic composition, either in the bulk melt due to an off-eutectic feed or at the freezing interface because of departure from the extremum condition.
3. Presence of a strong habit modifying impurity whose concentration at the freezing interface would be altered by convection.

At the beginning of the present grant, we favored the first of these hypotheses and set out to test it both experimentally and theoretically. We planned the following approaches:

1. Pass electric current pulses through the MnBi/Bi eutectic during directional solidification in order to produce an oscillatory freezing rate.
2. Directionally solidify the MnBi/Bi eutectic on Mir using the QUELD II gradient freeze furnace developed by Professor Smith at Queen's University.
3. Select another fibrous eutectic system for investigation using the Accelerated Crucible Rotation Technique to introduce convection.
4. Develop theoretical models for eutectic solidification with an oscillatory freezing rate.

Because of the problems with Mir, we substituted ground-based experiments at Queen's University with QUELD II vertical and horizontal, with and without vibration of the furnace. The Al-Si system was chosen for the ACRT experiments.

Three related approaches were used to model eutectic solidification with an oscillatory freezing rate. A sharp interface model was used to calculate composition oscillations at the freezing interface in response to imposed freezing rate oscillations. The resulting changes in supersaturation and undercooling were used to predict microstructure transformations due to nucleation.

Another model was based on the principle of minimum entropy production. We calculated the steady state and stationary periodic entropy production for eutectic systems. Expressions were found for spacing λ for growth at a constant freezing rate, oscillatory growth, and with a modulated freezing interface.

The third approach used the phase-field method to track the evolution of eutectic microstructure. It successfully displayed phenomena causing microstructure variation, including nucleation, lamella termination, oscillatory instability, irregular growth, and banding. The understanding of the mechanisms responsible for the change of the microstructure allowed us to explain the evolution of the microstructure in an oscillating temperature field.

All three models predicted a decrease in λ when the freezing rate oscillates in the absence of convection. Increasing freezing rate oscillations cause the average interfacial composition to depart increasingly from the eutectic composition.

An extensive series of experiments were performed on the MnBi/Bi eutectic. Continuous electric current had little effect on the microstructure of the eutectic. At translations rates >2 cm/hr, current pulses caused less of the ingot to have a quasi-regular microstructure. Without current, the volume fraction of MnBi in the quasi-regular regions ranged from 3% to 4%, compared to the theoretical value for the eutectic of 3.15%. The volume fraction of MnBi increased with increasing current pulsing amplitude. The average rod spacing decreased with increasing current amplitude and increasing duration time. Negative current pulsing had less effect on the microstructure than did a positive current. The QUELD II experiments failed to show effects of ampoule orientation or vibration, but did indicate that the freezing rate reached a maximum part way down each ingot. The position of this maximum varied from ingot to ingot.

Twenty-five Al-Si eutectic ingots were grown by the vertical Bridgman-Stockbarger technique. Some were solidified during application of the Accelerated Crucible Rotation Technique (ACRT) in order to generate convection. Some ingots had 0.01 wt% Sr added as a silicon habit modifier, which tends to convert the silicon from flakes to rods. The scatter in the data did not permit any firm conclusions on the influence of ACRT on the microstructure, although the apparent effect of ACRT varied along the length of the ingot. This could indicate that the strong convection caused by ACRT caused the composition and doping of the alloy to vary during solidification, leading to a variation in microstructure.

These results do not favor our original hypothesis. Instead, they indicate that departure of the interfacial composition from the eutectic may be making the microstructure sensitive to convection. Although this departure can arise from the failure of the eutectic to freeze at the extremum, our modeling showed that an oscillatory freezing rate also gives rise to a change in interfacial composition. Thus, irregular convection may cause a change in microstructure both by causing a fluctuating freezing rate and by altering the composition field near the freezing interface.

One paper has been published resulting from this research. Four others have been written and are being polished for submission to refereed journals. Two MS and one PhD thesis are nearing completion.

Acknowledgments We are very grateful to Ms. Barbara Facemire for her interest and encouragement, and for arranging use of the supercomputer at Marshall Space Flight Center. Without this assistance, the very interesting phase-field results would not have been possible. We thank Professor Reginald Smith at Queen's University for suggesting study of the Al-Si eutectic and for arranging for experiments to be performed in QUELD II. Ms. Carolyn Russell was immensely helpful in performing those experiments. Mr. Craig Burkhard assisted in the Al-Si work.

Availability of CD-ROM Our theoretical analyses have producing several very interesting time-dependent results that cannot be fully appreciated from still photos. A CD-ROM showing these results is available upon request to Professor Regel.

CONTENTS

THE INFLUENCE OF A FLUCTUATING FREEZING RATE ON DIRECTIONAL SOLIDIFICATION OF THE MnBi/Bi EUTECTIC

Fengcui Li

Abstract

The objective of this project is to determine the effect of a fluctuating freezing rate on the microstructure of the MnBi/Bi eutectic. It was planned that this would be done via both microgravity experiments and ground-based experiments. The microgravity experiments were to be carried out in collaboration with Professor Reginald Smith of Queen's University. Through the support of the Canadian Space Agency, he had two automated furnaces located in the Canadian Microgravity Isolation Mount (MIM), in Prirorda on Mir. Because of problems with Mir, we were unable to perform these experiments. Gradient freeze experiments at Queens on a duplicate of the flight furnace showed that the freezing rate varied along the ingot in a non-reproducible manner.

At Clarkson, ground-based experiments are being performed with a fluctuating freezing rate caused by passing periodic electric current pulses through the material. Continuous electric current had little effect on the microstructure of the eutectic. At translations rates >2 cm/hr, current pulses caused less of the ingot to have a quasi-regular microstructure. Without current, the volume fraction of MnBi in the quasi-regular regions ranged from 3% to 4%, compared to the theoretical value for the eutectic of 3.15%. The volume fraction increased with increasing current pulsing amplitude. The average rod spacing decreased with increasing current amplitude and increasing duration time. Negative current pulsing had less effect on the microstructure than did a positive current.

Experimental methods

The MnBi-Bi eutectic was directionally solidified using a vertical Bridgman-Stockbarger apparatus at Clarkson University. The experimental methods were described in the March 1998 annual report. Seven initial experiments were performed with the freezing rate or electric current pulsing conditions changed at intervals during each run. As discussed below, this provided inconclusive results. Subsequently, seven sets of experiments were performed. Each set consisted of four ingots solidified at the same ampoule translation rate (1.1 to 9.8 cm/hr), but with different electric current conditions. One ingot was solidified with no current, one with 40 A/cm^2 of current passed continuous through it, one with periodic positive current pulses[1], and one with negative current pulses. In a pulsing experiment, the current was suddenly turned on, held constant for time t, and then turned off. Here, the period is denoted by the letter T.

The microstructure in cross-sectional slices was photographed under the scanning electron microscope. The resulting digital images were analyzed using HLImage++ software to yield the number of rods, and the area, center coordinates and roundness of each rod. From these data, the rod density (ρ) and the area fraction (f) of MnBi were calculated. The nearest neighbor distance λ of each rod was calculated from the distance of its center to that of its nearest neighbor. The average λ, its standard deviation SD, kurtosis, and skewness and 95% confidence limits were obtained with the statistical analysis software in Microsoft Excel™. Each ampoule was

[1] Positive electric current is defined as the electric current passing from the solid to the melt.

used in the experiments: no current, 40 A/cm^2 continuous electric current, positive current pulses and negative current pulses. In the pulsing experiment, the current was suddenly turned on, held constant for time t, and then turned off. The period was time T.

Solidification with different translation rates along the ingot

In order to test the effect of translation rate on the microstructure of MnBi/Bi eutectic, two ingots were solidified with changes in the translation rate during each run. Ingot number 3 was solidified with four translation rates; the first 4.5cm at 6.8cm/hr, 3.0cm at 4.1cm/hr, 3.0cm at 2.1cm/hr, and the last 2.0cm at 0.83cm/hr. The average rod spacing λ at 5 mm intervals is shown in Figure 1, along with the presumed translation rates. There was a quasi-regular rod structure throughout. Unfortunately, it was not possible to tell where the changes in freezing rate occurred because the position of the freezing interface in the furnace is unknown. And, of course, it is recognized that the freezing rate does not instantly assume a new translation rate. Rather it approaches the new rate asymptotically as the freezing interface shifts to a new steady state position in the furnace. Similar results were obtained with ingot number 4.

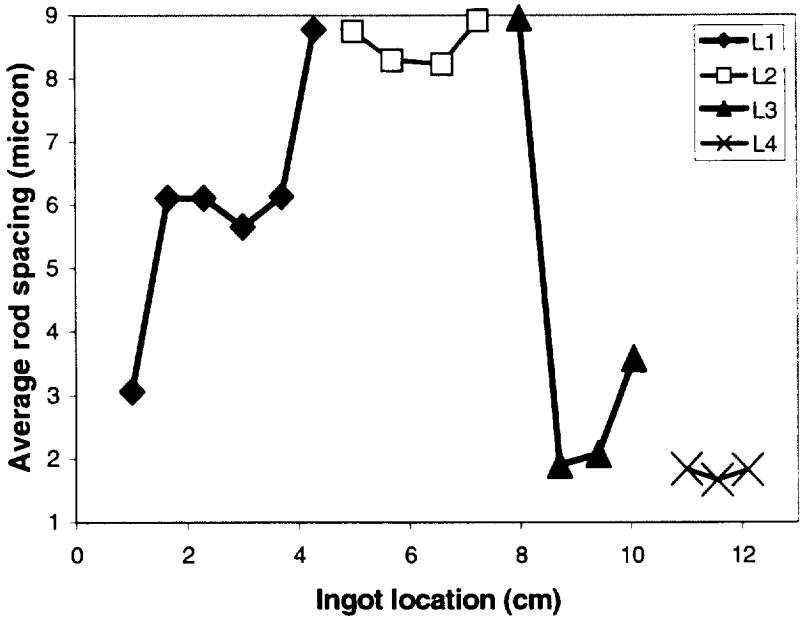

Figure 1. Average rod spacing λ along the ingot number 3. Guessed translation rates: L1: V=6.8cm/hr; L2: V= 4.1cm/hr; L3: V=2.1cm/hr; L4: V=0.83cm/hr

Solidification with different current pulsing conditions

Ingots 5, 6 and 7 were solidified with the current pulsing conditions changed at intervals along each ingot. Ingot number 5 was solidified at a translation rate of 2.1 cm/hr with positive current pulses of duration time t = 0.75s and period T = 6s. The first 4cm was solidified without current, then 3.5cm with 9.0A current pulses, 3.5cm with 5A, 3.5cm with 1A, and the last 3.3cm without current. The result is shown in Figure 2. Again, it was not possible to tell where exactly the changes in current density had been made. Nonetheless, we used sections A, B, C, and D to estimate λ versus freezing rate, as shown in Figure 3. Similar results were obtained with ingot

number 6. Ingot number 7 was not analyzed because these results seemed unclear and, furthermore, were contrary to our predictions and to Dr. Cai's preliminary results using the same technique. In order to try to find the exact position of the solid-melt interface, ingot number 8 was solidified with larger current densities to demarc the interface at intervals. This was not successful.

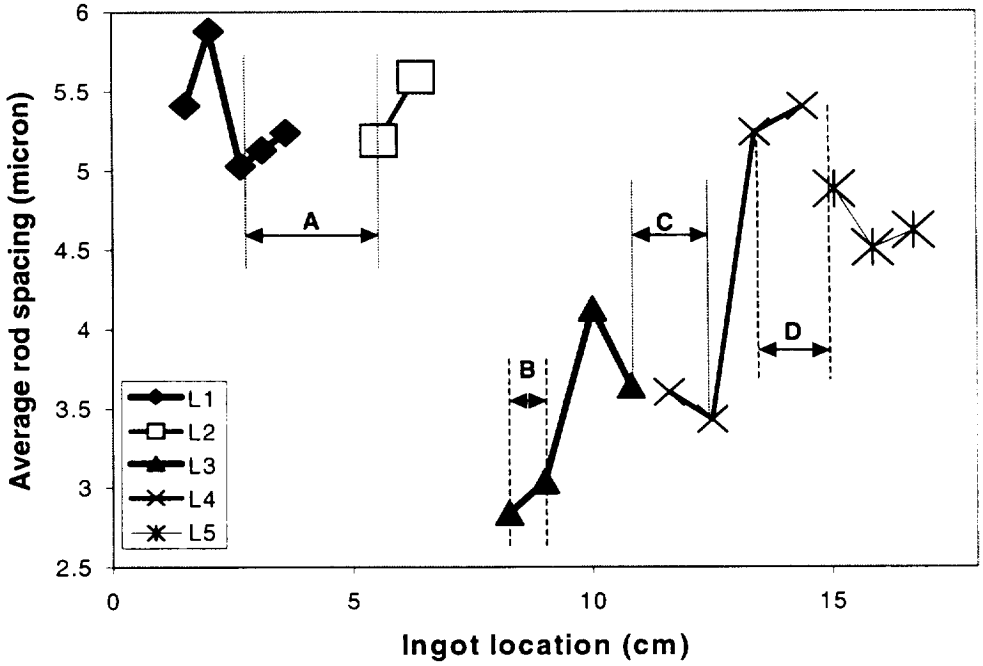

Figure 2. Average rod spacing λ along the ingot number 5, with guessed current amplitudes of:
L1 and L5: no current; L2: 9A pulses; L3: 5A pulses; L4: 1A pulses

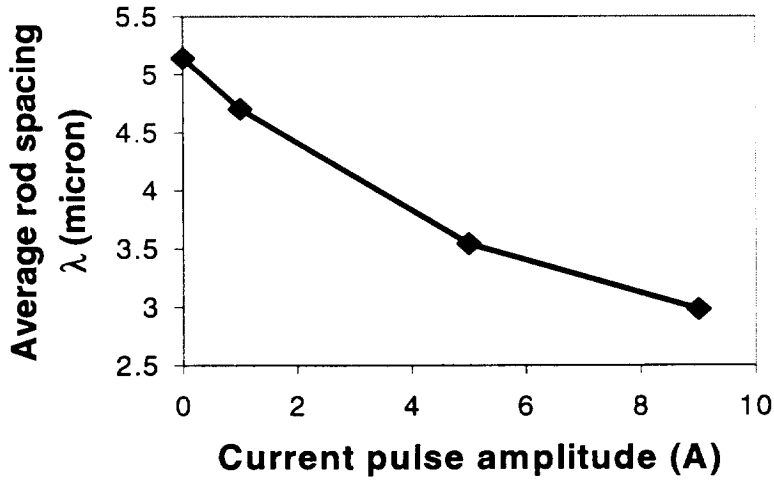

Figure 3. Average rod spacing λ versus current pulse amplitude in ingot number 5 using sections A, B, C and D shown in Figure 2.

Solidification with constant conditions

To avoid the above uncertainties in the conditions under which each section of an ingot was grown, subsequent experiments were performed with constant freezing rate and current pulsing conditions for each ingot. Each ingot length was about 7.2cm. The slices in all 5 ingots were cut at the same time to insure that they were at the same positions in each ingot, as shown schematically in Figure 4. For each cross section, 11 SEM images were taken at different locations. An average rod spacing was computed from the rod spacings in all these images.

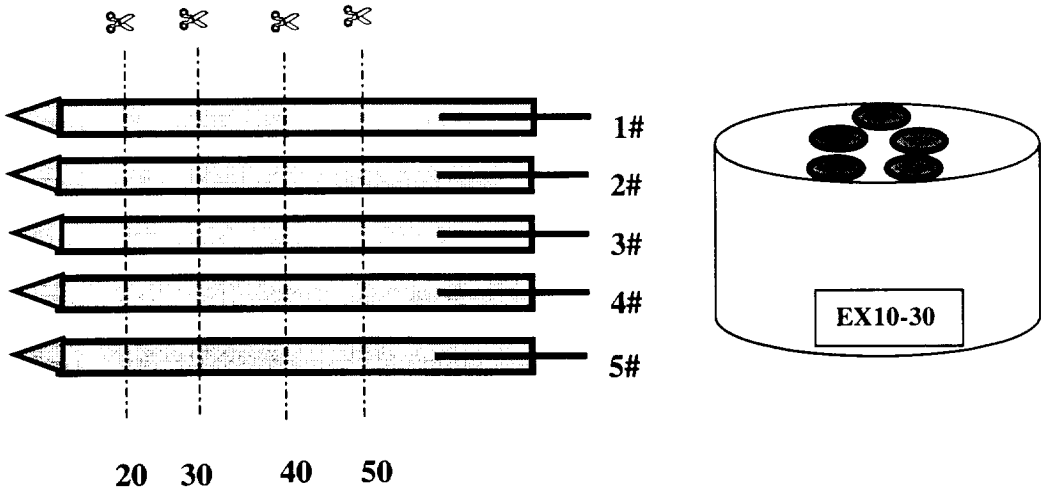

Figure 4. Schematic diagram of the cutting and mounting of five ingots from a set of experiments.

Influence of growth conditions on the types of microstructure

Several types of microstructures were observed, depending on the freezing rate and current pulsing conditions. The usual quasi-regular MnBi rod structure is shown in Figure 5, with mostly triangle or chevron cross sections. As the current amplitude or duration was increased, regions with other microstructures appeared, as shown in Figure 6. The MnBi in these regions was coarse and irregular, large rods, broken lamellae, or rod clusters. In some, the MnBi was missing altogether. For example, with V = 2.1cm/hr translation rate, 72 A/cm^2 positive current pulses, t = 4.5s current pulse duration time and T = 18s period, the fraction of the ingot with a quasi-regular structure was only 34%. At a freezing rate of 2.1 cm/hr and above, the microstructure became less regular as the current density was increased. The opposite behavior was true at a freezing rate of 1.1cm/hr, which is at the boundary between irregular microstructures at lower freezing rates and quasi-regular at higher rates. The percent with a quasi-regular microstructure is shown at Figure 7.

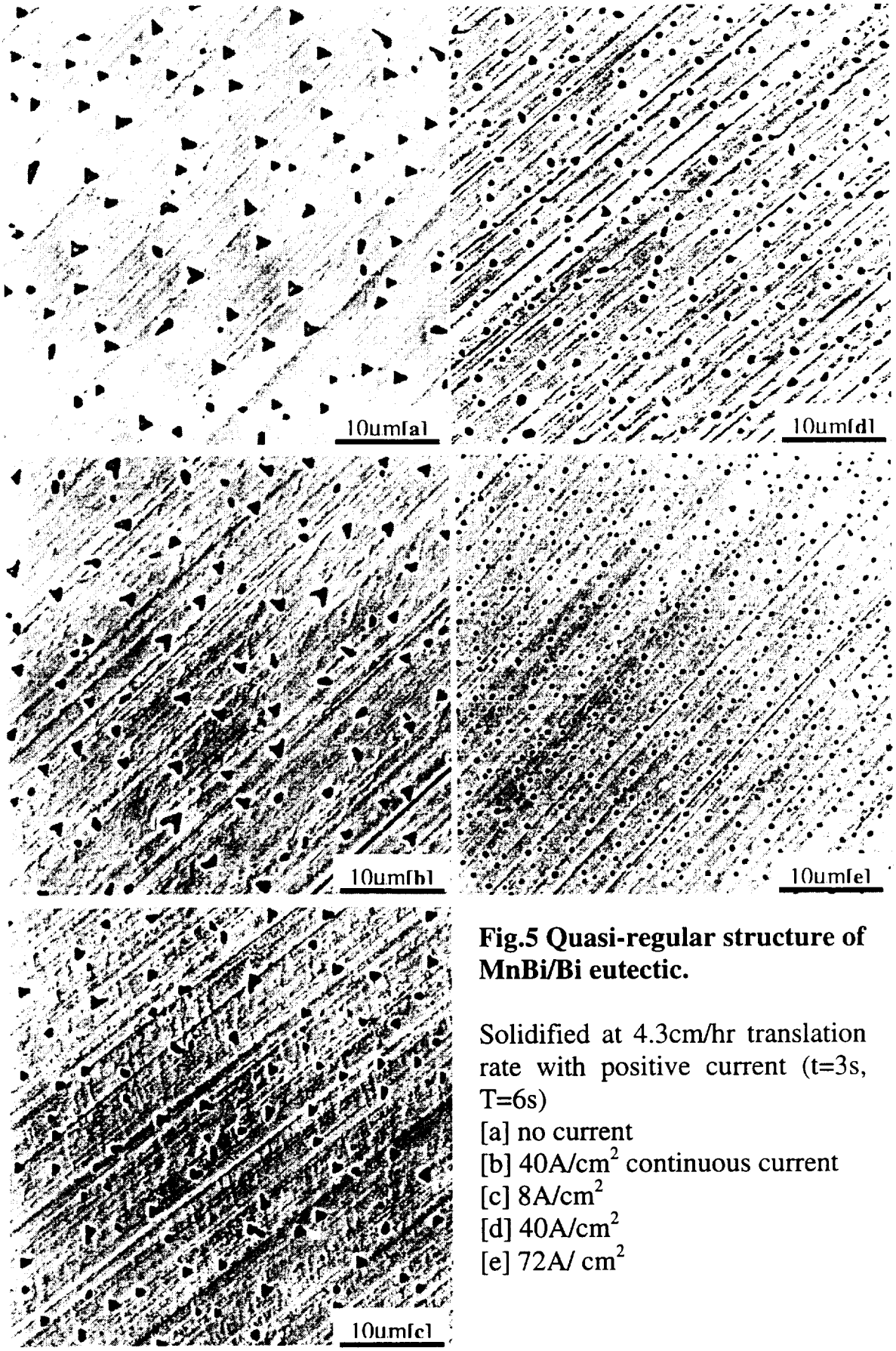

Fig.5 Quasi-regular structure of MnBi/Bi eutectic.

Solidified at 4.3cm/hr translation rate with positive current (t=3s, T=6s)
[a] no current
[b] 40A/cm^2 continuous current
[c] 8A/cm^2
[d] 40A/cm^2
[e] 72A/ cm^2

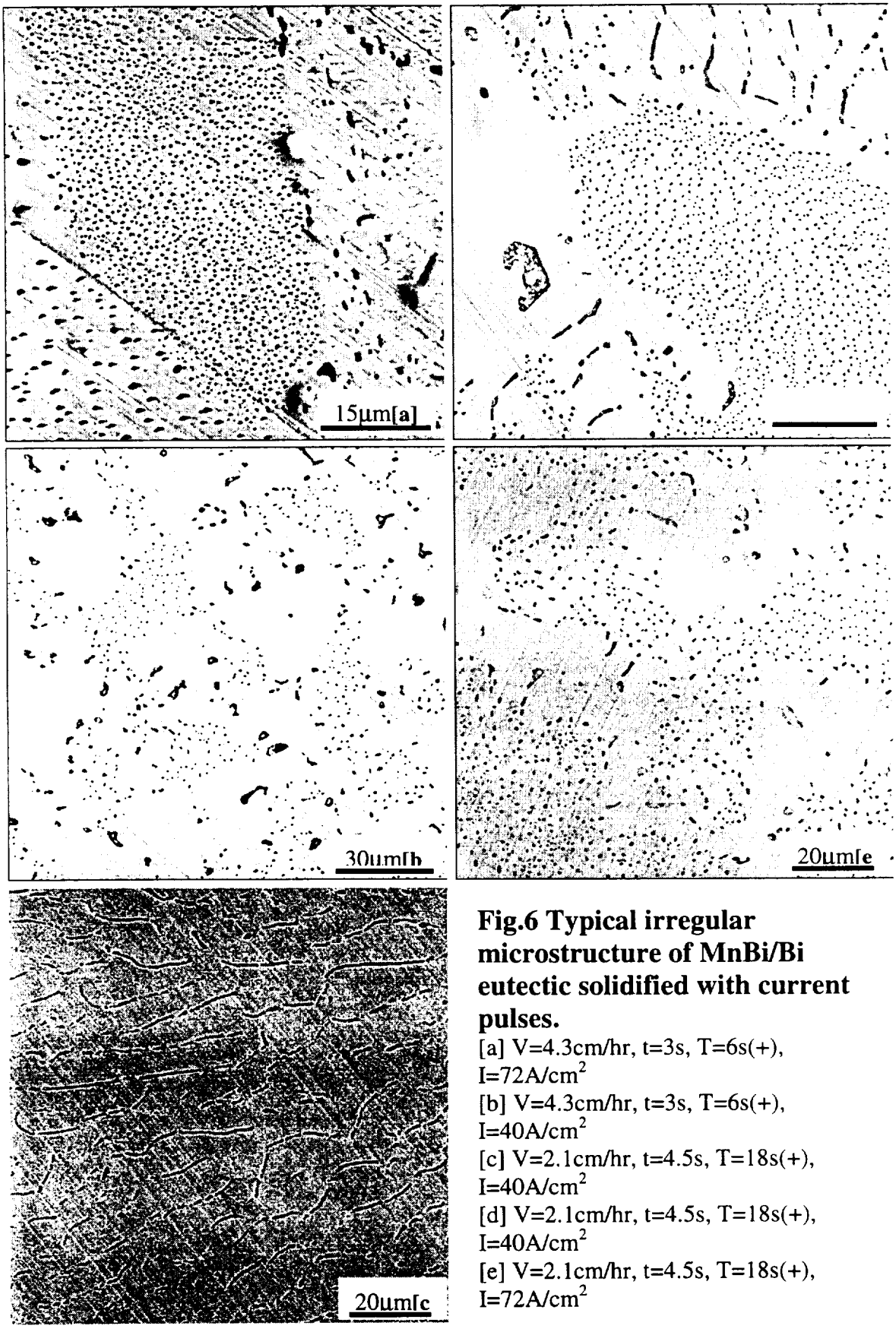

Fig.6 Typical irregular microstructure of MnBi/Bi eutectic solidified with current pulses.

[a] V=4.3cm/hr, t=3s, T=6s(+), I=72A/cm^2

[b] V=4.3cm/hr, t=3s, T=6s(+), I=40A/cm^2

[c] V=2.1cm/hr, t=4.5s, T=18s(+), I=40A/cm^2

[d] V=2.1cm/hr, t=4.5s, T=18s(+), I=40A/cm^2

[e] V=2.1cm/hr, t=4.5s, T=18s(+), I=72A/cm^2

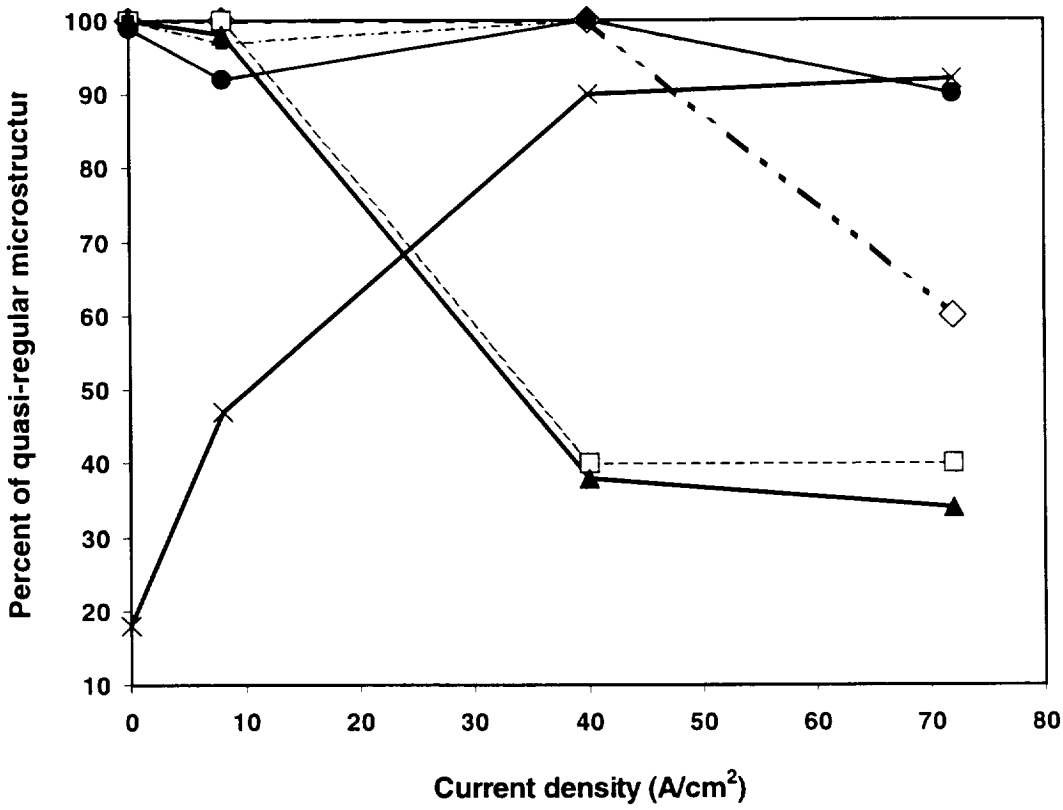

Figure 7. Percent of quasi-regular microstructure in cross section versus current density.

◇: V=2.1cm/hr, t=0.75s, T=6s(+)
□: V=4.3cm/hr, t=3s, T=6s(+)
▲: V=2.1cm/hr, t=4.5s, T=18s(+)
×: V=1.1cm/hr, t=0.25s, T=2s(+)
●: V=5.5cm/hr, t=3s, T=6s(-)
■: V=4.4cm/hr,t=3s,T=6s(-)

Rod spacing

For the portions with a quasi-regular rod structure we determined the average nearest neighbor distance (λ), rod density (ρ) and the area fraction (f) of MnBi, as discussed earlier. The 95% confidence limits were about $\pm 1.5\%$ of the value of λ. The standard deviation was almost 1/3 of λ, as shown in Figure 8. The kurtosis and skewness were less than one standard deviation. From a plot of the ratio of kurtosis to standard deviation versus the ratio of skewness to standard deviation (Figure 9), we concluded that the rod spacing was normally distributed, except for one ingot solidified without current at 1.1 cm/hr translation rate, and two ingots solidified with large current amplitude at translation rates larger than 2cm/hr.

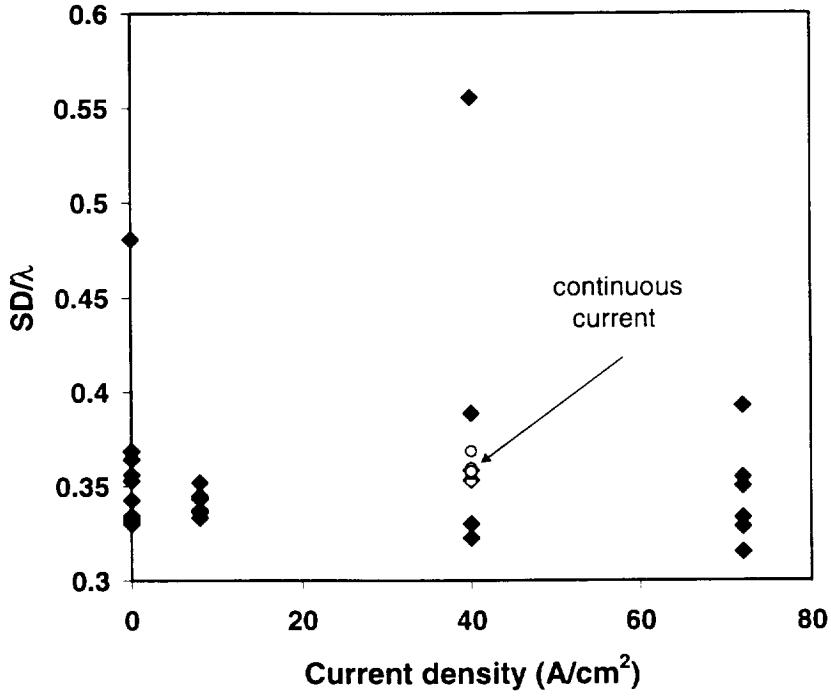

Figure 8. Ratio of standard deviation SD of nearest neighbor distances to average λ versus current density in the quasi-regular portions of all ingots.

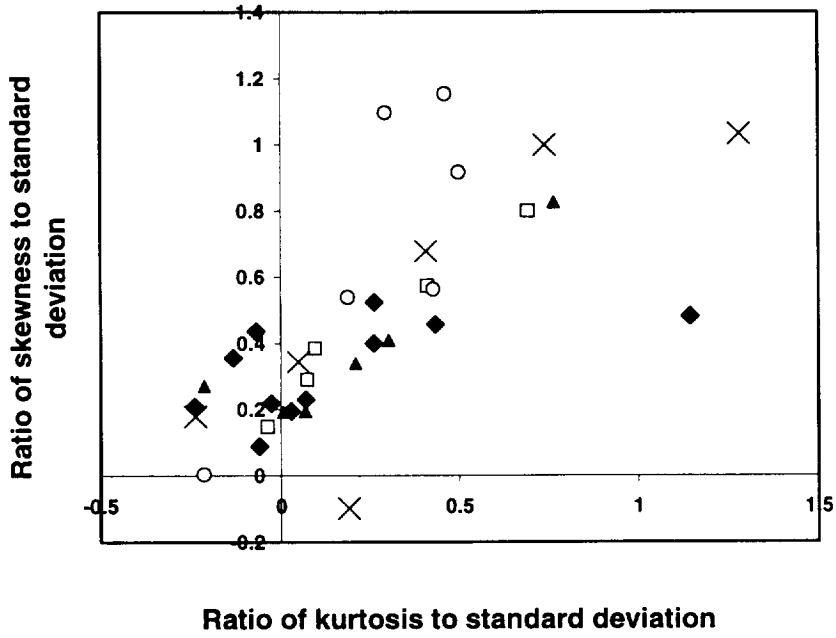

Figure 9. Ratio of skewness to standard deviation versus ratio of kurtosis to standard deviation.

Variation in λ along the ingots

Figure 10 shows the average nearest neighbor distance λ versus position for two ingots solidified at V = 2.1cm/hr, with and without current pulsing. Shown are both the λ determined as above and another estimate of rod spacing, the inverse square root of the rod density ρ. The trend of $1/\rho^{0.5}$ is the same as for λ, but $1/\rho^{0.5}$ is ~2 μm larger than λ, reflecting the irregular spacing of the rods. The largest difference of the four cross section averages is 0.16 μm, which is about 3% of λ. This shows that the average rod spacing along the ingot was relatively constant. The same results were obtained in other ingots. From these results we conclude that the freezing rate was constant during solidification, except for the perturbations introduced by current pulsing.

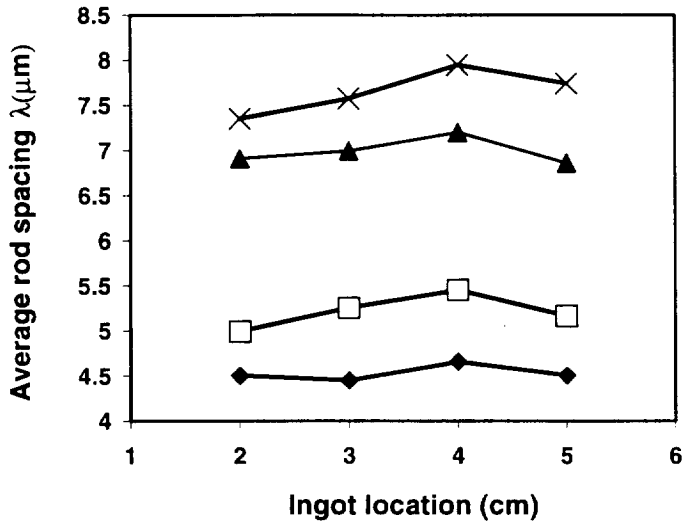

Figure 10. Average rod spacing along two ingots solidified at 2.1cm/hr.
◆: λ with I=8A/cm^2, t=4.5s, T=18s(+) □: λ without current pulsing
▲: $1/\rho^{0.5}$ with I=8A/cm^2, t=4.5s, T=18s(+) ×: $1/\rho^{0.5}$ without current pulsing

Influence of translation rate

Figure 11 shows λ versus the translation rate V on a log-log scale. The straight line is for a -1/2 slope, yielding $\lambda^2 V = 1.4\times10^{-16}$ m^3/s.

Influence of translation rate and electric current on the volume fraction of MnBi

The area fraction f of MnBi rods versus the translation rate V is shown in Figure 12, for eutectic solidified without electric current and with continuous current. The values strongly depend on the settings used in the image analyses. When a rod's image is over threshold, the rod area is a little larger than its true value. The difference in area between the under threshold and over threshold values is about 0.7%. We conclude that the translation rate has little effect on the volume fraction of MnBi, while continuous current increased it slightly. Figure 13 shows that the volume fraction of MnBi increased with increasing current density.

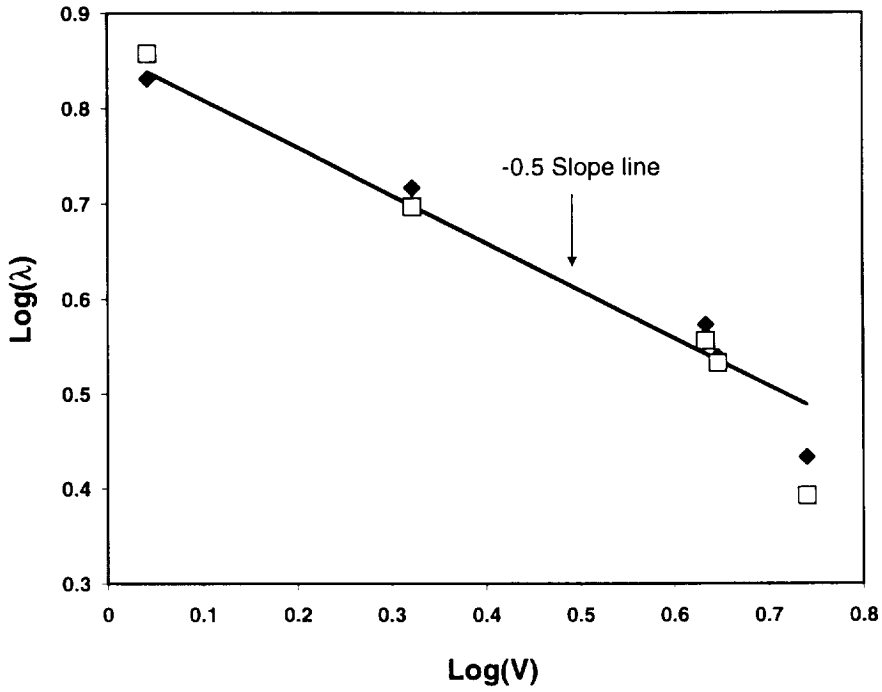

Figure 11. The average rod spacing λ in μm versus translation rate V in cm/hr.
◆: without current □: with continuous current

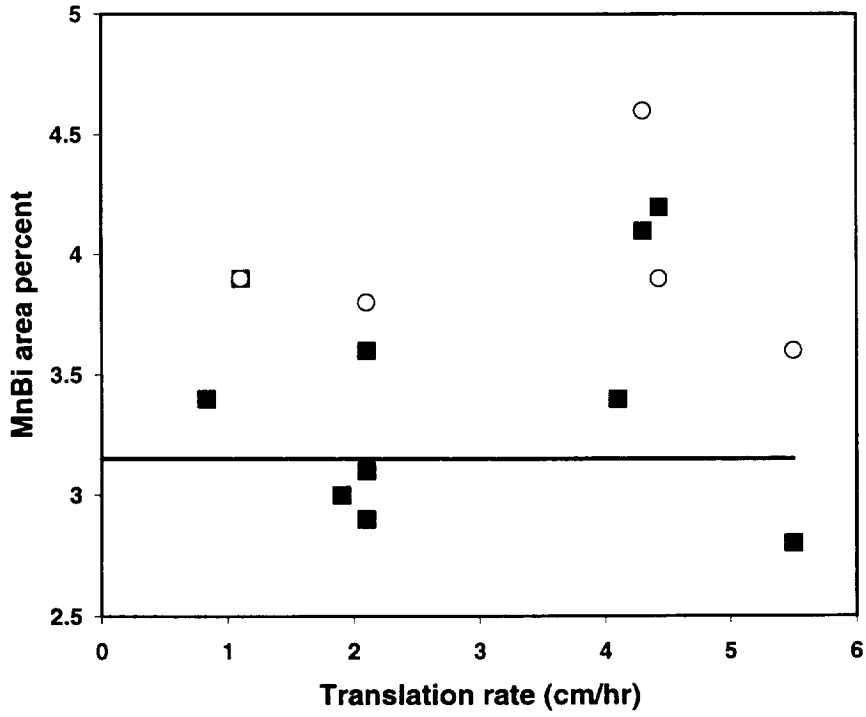

Figure 12. Area percent MnBi fibers versus translation rate.
◆: without current ○: continuous current

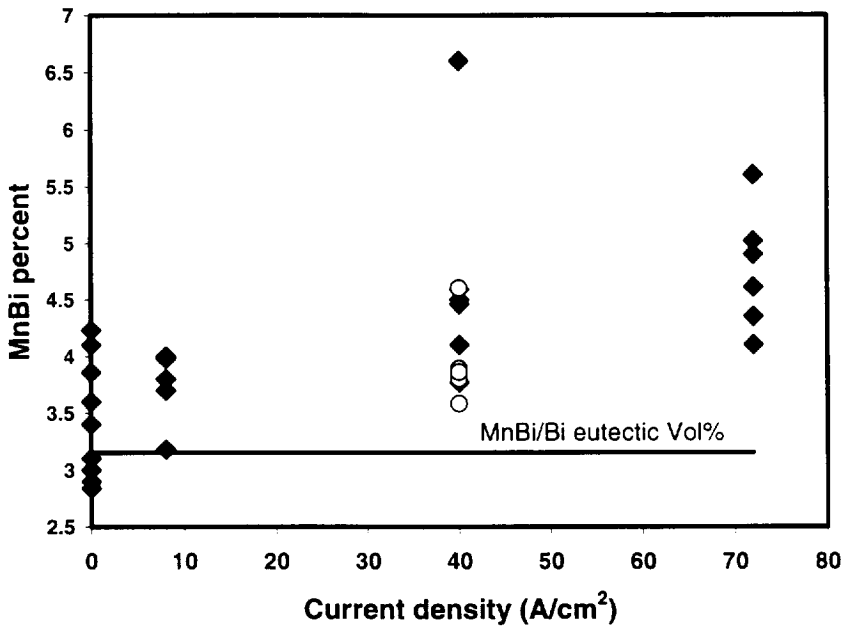

Figure 13. Area percent of MnBi versus current density for quasi-regular structure.

○: continuous current ◆: without current

Influence of electric current pulsing on MnBi rod spacing

Figure 14 shows the average rod spacing λ versus the current density of three sets of experiments with positive current pulsing. The average rod spacing without current was almost the same as that solidified with constant current. When the material was solidified with current pulses, λ decreased with increasing current amplitude. Two ingots were solidified with negative current, i.e. from the melt to the solid. The results are shown in Figure 15. Continuous negative electric current had little effect on the microstructure, while current pulsing decreased λ, although less than with positive current. Figure 16 shows results for two experiments with the same solidification conditions (4.3~4.4 cm/hr, 3s duration time and 6s period) except for current polarity. The average rod spacing decreased 46% when the material was solidified with 72 A/cm^2 positive current pulses. Figure 17 shows the fraction of MnBi in regions with a quasi-regular microstructure in these two ingots.

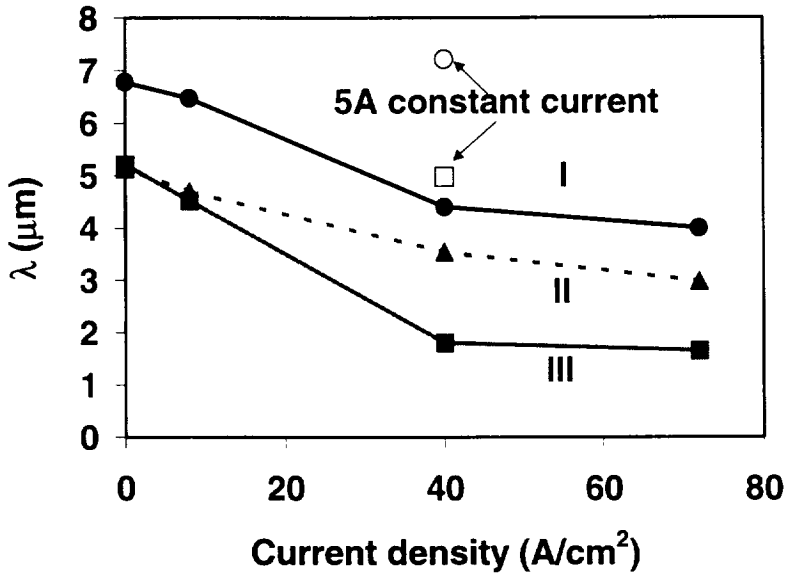

Figure 14. Average rod spacing λ versus current density.
I ●: V=1.1cm/hr, t=0.25s, T=2s(+);
II ▲: V=2.1cm/hr, t=0.75s, T=6s(+);
III ■: V=2.1cm/hr, t=4.5s, T=18s(+)

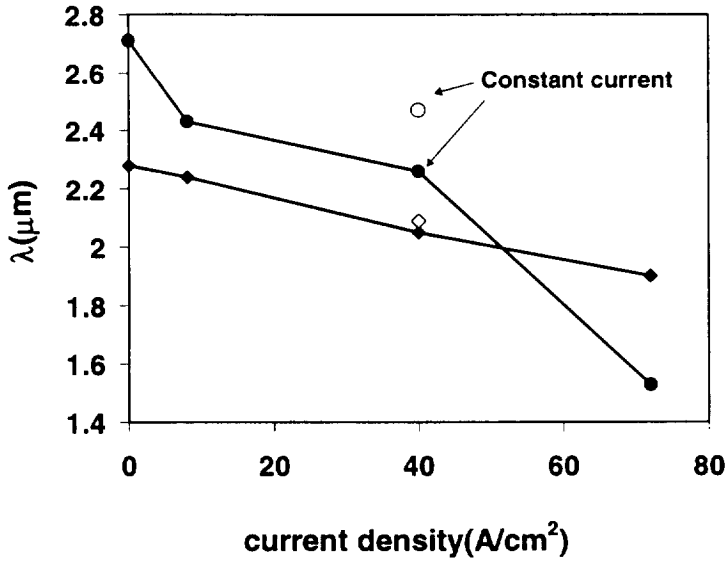

Figure 15. Average rod spacing λ versus current density for negative current.

◆: V=8.0cm/hr, t=3s, T=6s(-) ● : V=5.5cm/hr, t=3s, T=6s(-)

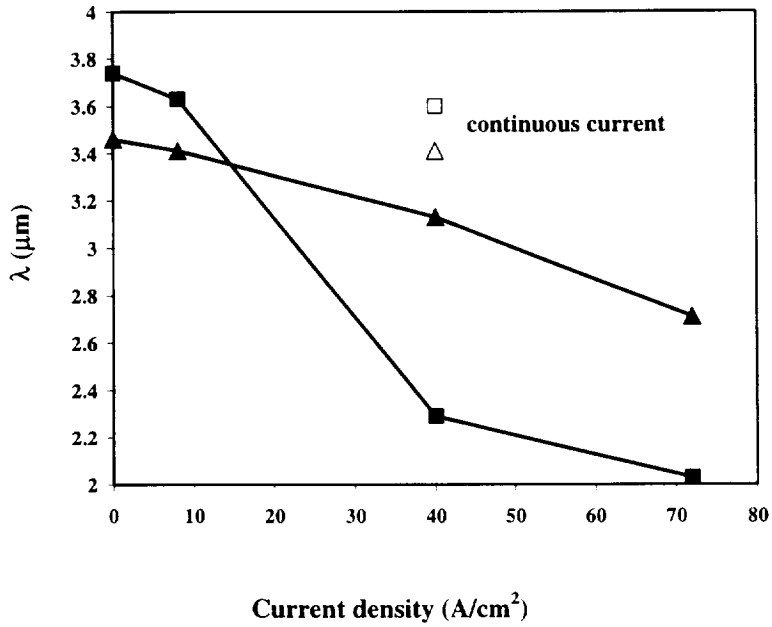

Figure 16. The effect of electric current polarity on λ.
■: V=4.3cm/hr,t=3s, T=6s(+) ▲: V=4.4cm/hr, t=3s, T=6s(-)

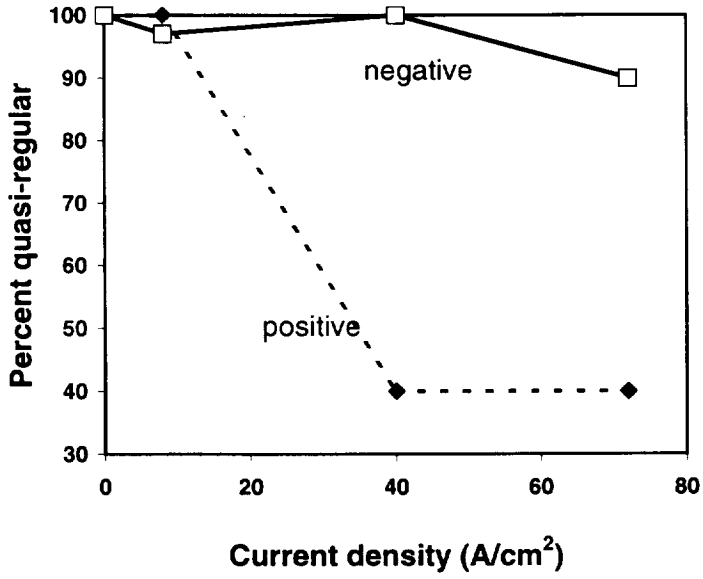

Figure 17. The effect of electric current polarity on the regularity of the microstructure.

QUELD II experiments

Twelve MnBi/Bi eutectic ingots were solidified in the QUELD II ground based unit at Queen's University. The diameter of the ingots was 3mm. The ingots were solidified horizontally and vertically and with three vibration conditions: no vibration, 0.5 Hz and 1.0 Hz; and at 0.71°C/min and 2.86°C /min cooling rates, yielding ~1.0cm/hr and ~3.5cm/hr freezing rates. Each quartz ampoule was ~6 cm long with ~4.5 cm long charges. The ingots' lengths were 3.0 to 3.7 cm long after solidification.

As shown in Figure 18, the microstructure of the ingots solidified vertically was more regular than those solidified horizontally. The MnBi rods had a wider variety shapes when the eutectic was solidified horizontally. As shown in Figure 19, those solidified without vibration had a more regular microstructure than those solidified with vibration. Figure 20 shows the percents of the ingots with a quasi-regular microstructure. Figure 21 shows average rod spacings along each ingot.

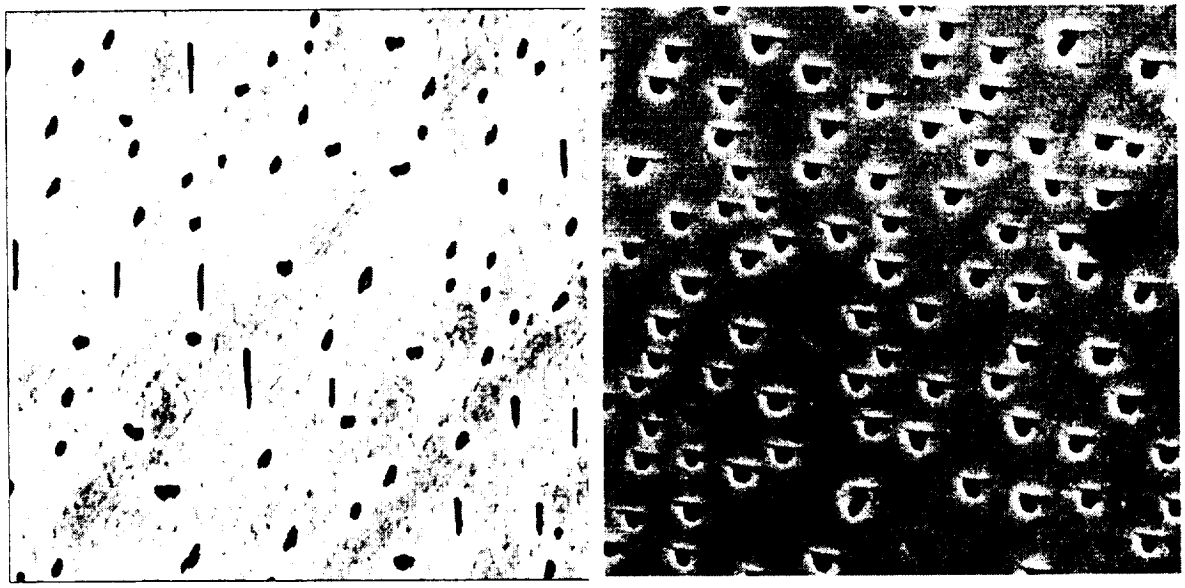

A: 2.86°C/min cooling rate, horizontal, without vibration (4000X)

B: 2.86°C/min cooling rate, vertical, without vibration(6000X)

Figure 18. The microstructure of MnBi/Bi eutectic solidified in QUELD II vertically upward and horizontally, without vibration.

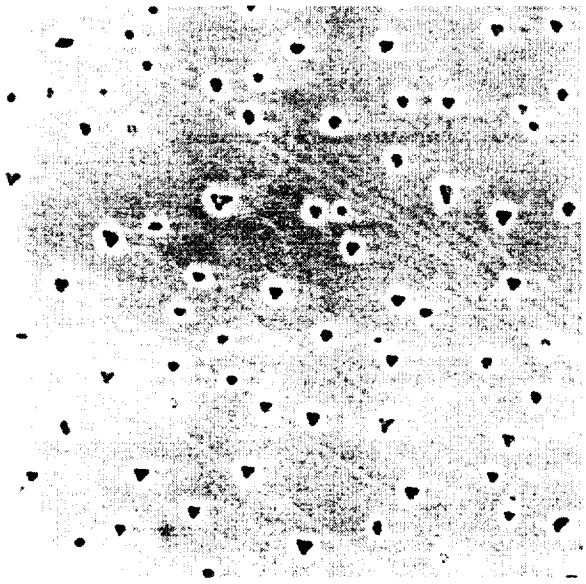

A: 0.71°C/min cooling rate, without vibration, vertical (2000X)

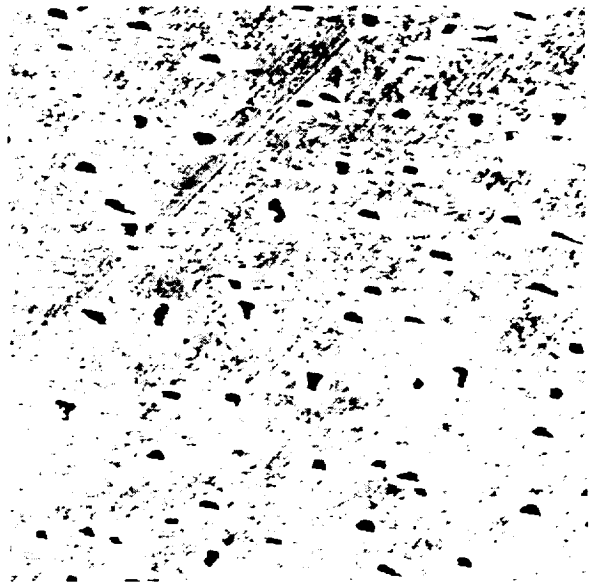

B: 0.71°C/min cooling rate, with 0.5 Hz vibration, vertical (2000X)

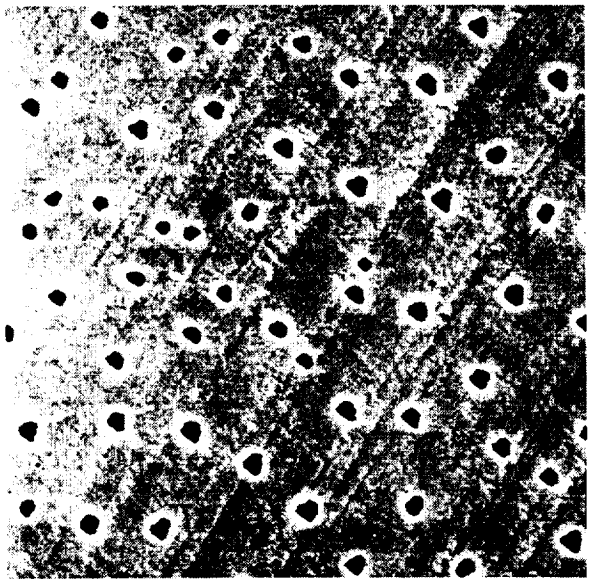

C: 2.86°C/min cooling rate, without vibration, vertical (4000X)

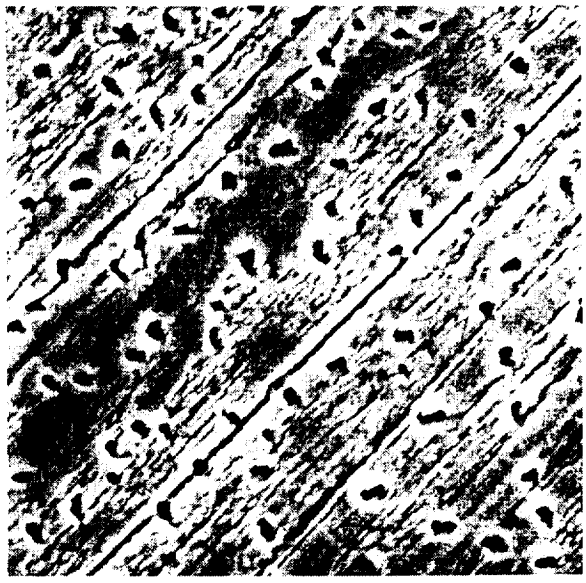

D: 2.86°C/min cooling rate, without vibration, vertical (5000X)

Figure 19. The microstructure of MnBi/Bi eutectic solidified in QUELD II with and without vibration

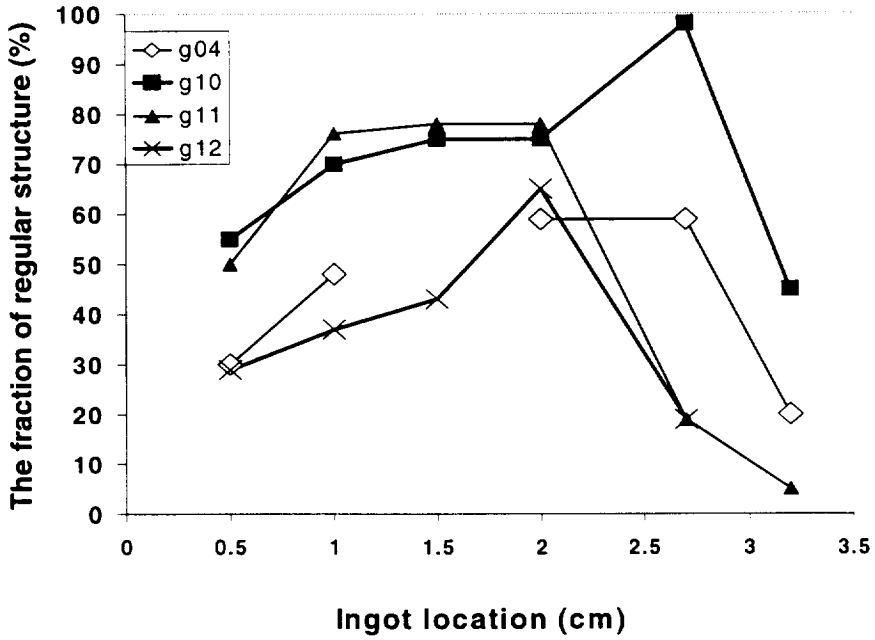

Figure 20a. Percent of ingots solidified horizontally with quasi-regular microstructure (V=3.5cm/hr) (G11, G12: without vibration, G04: 0.5Hz, G10: 0.9Hz)

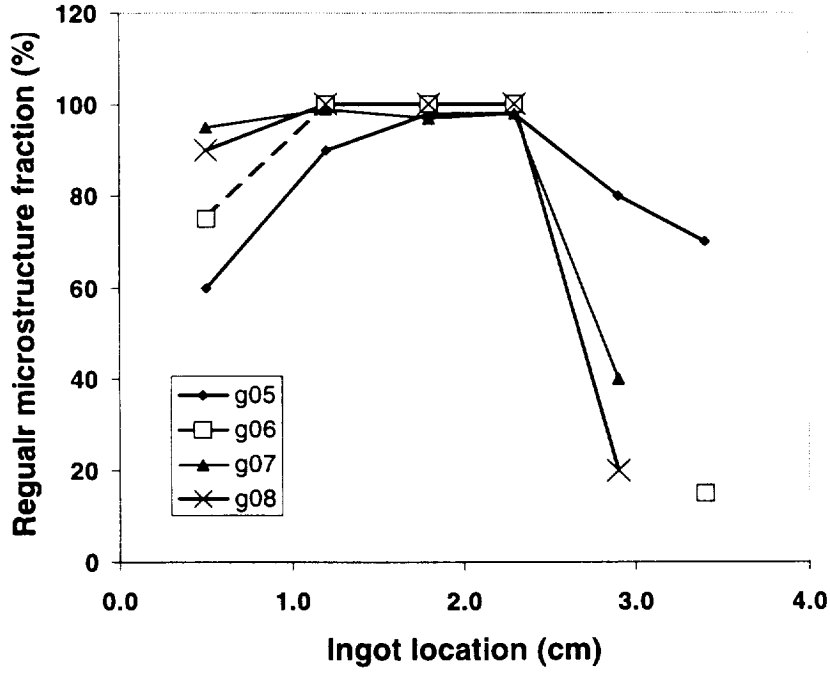

Figure 20b. Percent of ingots solidified vertically with quasi-regular microstructures (V=3.5cm/hr) (G05, G08: without vibration, G06: 0.5Hz, G07: 0.8Hz vibration)

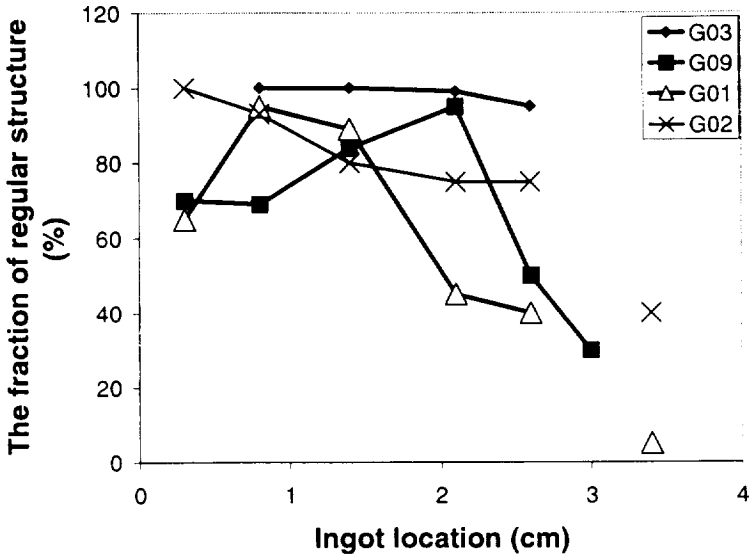

Figure 20c. Summary of percent of ingots with quasi-regular microstructure. V=1.0cm/hr (G01: horizontal, G02: horizontal, 0.5Hz vibration, G03: vertical, G09: vertical, 0.5Hz vibration)

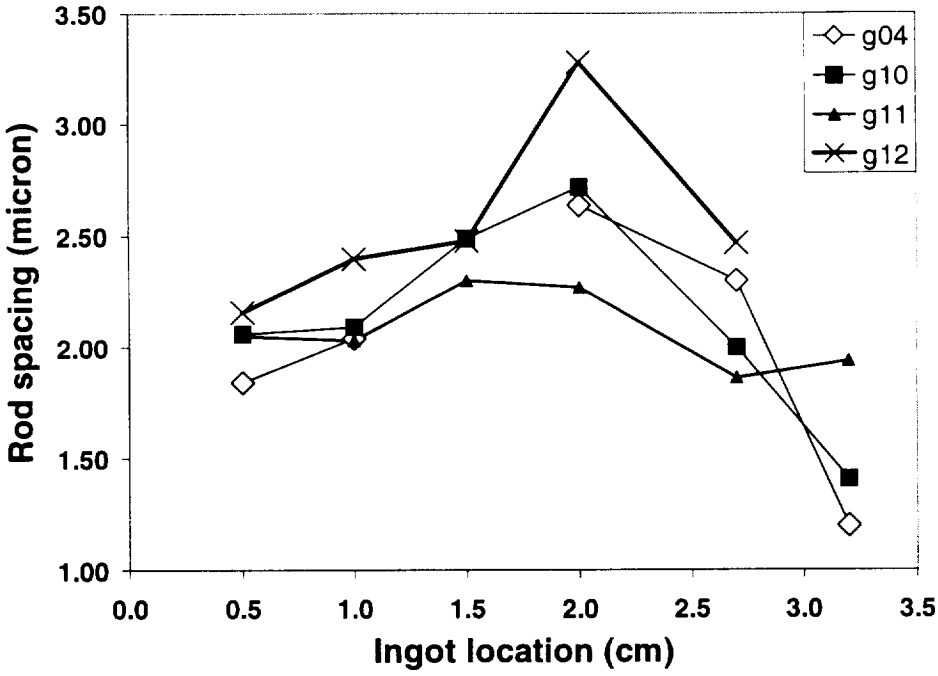

Figure 21a. Average rod spacing in ingots solidified horizontally (V=3.5cm/hr) (G11, G12: without vibration, G04: 0.5Hz, G10: 0.9Hz)

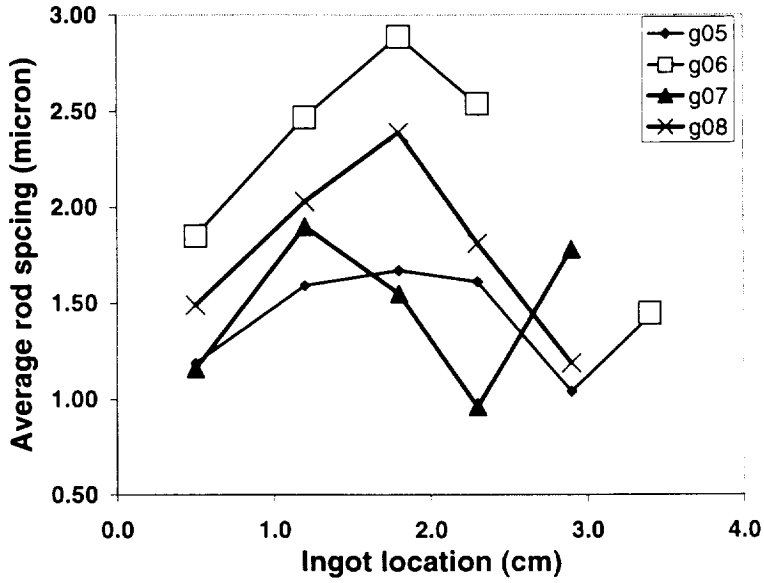

Figure 21b. Average rod spacing in ingots solidified vertically (V=3.5cm/hr) (G05, G08: without vibration, G06: 0.5Hz, G07: 0.8Hz vibration)

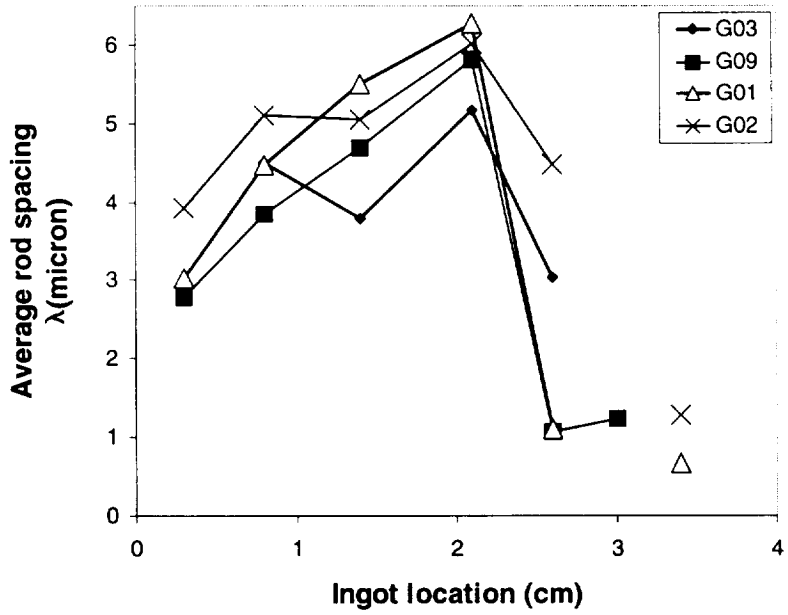

Figure 21c. Average rod spacings for ingots solidified at about 1.0cm/hr. G01: horizontal, G02: horizontal, 0.5Hz vibration, G03: vertical, G09: vertical, 0.5Hz vibration

DIRECTIONAL SOLIDIFICATION OF Al-Si EUTECTIC

Ramanathan Ramnarayanan

Abstract

The objective of this project was to determine the influence of convection during directional solidification on the microstructure of the Al-Si eutectic. About 25 ingots were grown by the vertical Bridgman-Stockbarger technique, with the material being contained in alumina crucibles inside sealed quartz ampoules. Some were solidified during application of the Accelerated Crucible Rotation Technique (ACRT) in order to generate convection. (We recognize that ACRT not only causes vigorous convection, but also causes the freezing rate to fluctuate [17].) Some ingots had 0.01 wt% Sr added as a silicon habit modifier, which tends to convert the silicon from flakes to rods. The scatter in the data did not permit any firm conclusions on the influence of ACRT on the microstructure, although its effect varied along the length of the ingot. This could indicate that the strong convection caused by ACRT causes the composition and doping of the alloy to vary during solidification, leading to a variation in microstructure.

Introduction

The aluminum-silicon eutectic is a widely studied faceted/non-faceted system that is commercially important, with numerous applications in foundry and casting industries. It is estimated that Al-Si alloys provide about 90% of all shaped castings. The reason for the wide study of Al-Si alloys arises from both its commercial applications as well as modification of its microstructure by addition of elements such as sodium and strontium in small quantities. Earlier [1,2,3,5,6,8,14] attempts to study impurity modification concerned themselves with complete modification, i.e., structures in which the Si phase was completely changed from a flake to a fibrous form. The primary impurity had been used in the past was sodium. Because sodium has a tendency to diffuse out of the ingot during aging is has been replaced by strontium, which has a greatly reduced tendency to diffuse out.

Clapham and Smith [9,10] were among the first to suggest the use of partial modification as a tool to determine the mechanism of impurity modification. They found that partially modified structures occur at solidification rates between 3.6 and 90 mm/hr, temperature gradients between 60-90°C/cm, and Sr concentrations between 0.004 and 0.014 wt%. The structure was sensitive to both the Sr level ahead of the solid/liquid interface and the freezing rate.

Our interest primarily lay in studying the effect of convection during solidification on the microstructure of the Al-Si eutectic. We obtained partially modified eutectics at a temperature gradient of 10K/cm and furnace translation rates that ranged from 10-80 mm/hr. The Sr concentration was 0.01wt%, which lies in the concentration range that yielded partially modified eutectics [10].

Experimental Methods

Alumina crucibles and quartz tubes were cleaned by various organic and inorganic solvents prior to loading the charge. The alumina crucible was rinsed with a slurry containing alumina particles. The purpose of the particles on the crucible wall was to prevent the ingot from sticking. The charge was put in the alumina crucible, which was then placed in a quartz tube sealed at the bottom end. This ampoule was evacuated for about 1 hour while gently heating with a H_2-O_2 torch from time to time to remove chemisorbed water. The ampoule was alternately evacuated and backfilled with Ar +10%H_2 gas at 10 psig. At the end of this flushing process, the quartz tube was sealed and placed inside the furnace.

Directional solidification and homogenization was carried out in a vertical Bridgman Stockbarger furnace (solid-down). The furnace was moved while the ampoule was held stationary, thereby avoiding any convection that might be caused by vibration of the ampoule in motion. The ampoule was held at the bottom, where a motor could be periodically turned on to cause rotation of the ampoule (ACRT). A hot zone temperature of 727^0C and a cold zone temperature of 450 ^{0}C were chosen, producing a temperature gradient of about 10^0C/cm. The melt was homogenized with the hot zone at 950^0C and cold zone at 900^0C. The ampoule was rotated at 100 rpm for 2 min, every 30 min. This process was carried out for 24 hours. The melt was then held at a hot zone temperature of 727^0C and a cold zone temperature of 450^0C for about 3-4 hours. At the end of this soak period, the translation unit was turned on. The translation rate was checked during each run. In an experiment involving ACRT, the timer was set to the on and off time intervals desired for the experiment.

After solidification, the samples were cut, mechanically polished, and examined with optical microscropy. The video camera attached to the microscope was connected to an image grabber board. The HLImage++ software was used to grab, digitize and analyze the images.

Results

About 25 ingots were grown. Some oxidized completely during growth, whereas others had only lightly oxidized surfaces. Three transverse cross-sections were taken from each ingot. Figure 1 shows a typical unmodified microstructure with aluminum dendrites (light) and flake Si (dark).

We did not employ the selective criteria reported in the literature [4,8,15] to characterize the microstructure. When selective criteria are used, one has to determine which portion of the sample has the most meaningful microstructure. In our approach to quantify the image, the specimen was slowly rotated till the flakes were vertical and coincided with the markings on the reticule of the microscope eyepiece. The distance between adjacent flakes was taken to be the eutectic spacing. If the flakes were bunched together, the eutectic spacing was taken as the distance from the first to the last as seen on the reticule divided by (n-1), where n represents the number of flakes. Dendritic spacing was determined in the same manner, except that the distance between the dendrite arms was taken to be the primary spacing. The distance between the adjacent smaller dendrites is reported here as the secondary spacing. The radius of the dendrites was taken to be half the diameter of the primary dendrite arm. These criteria are the same as those used by Trivedi and Kurz [16].

Figure 2 shows a partially modified microstructure.

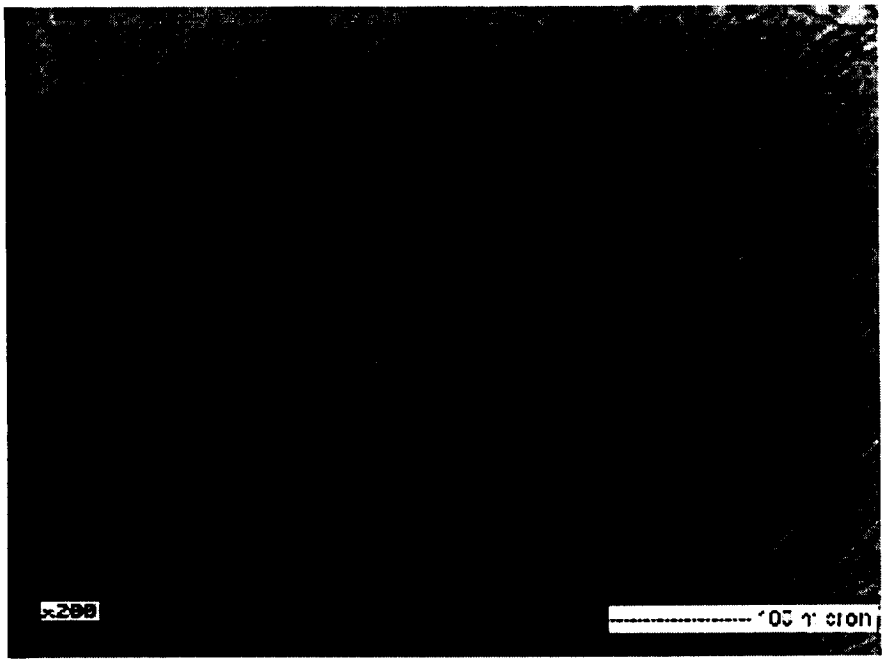

Figure 1. Transverse section cut 3.5 cm from the bottom of the ingot. Translation rate = 70mm/hr. Unmodified Al-Si. Ampoule Rotation rate = 80 rpm. Magnification 200X.

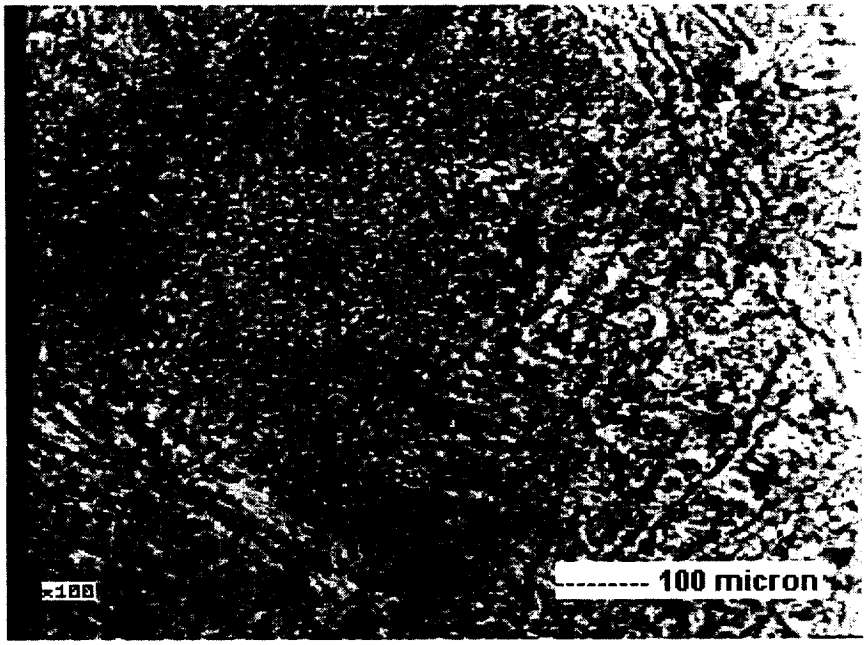

Figure 2. Transverse section cut 2 cm from bottom of the ingot. Translation rate = 10 mm/hr. Partially modified Al-Si. Magnification 100X.

We believe that we are the first to try and quantify such a microstructure. The fibrous Si appeared circular at magnifications from 200 to 1000x. Some spacings were taken by measuring the distance from the left edge of one fiber to the left edge of another. If the fibers were grouped together, the same approach as in flake Si was used. To check the accuracy of the software, some images were grabbed and spacing calculated using its blob analysis tool. The total number of fibers (N) and the total area (A) were used to define the eutectic spacing by $\lambda = 0.5\ (A/N)^{0.5}$. The error is estimated to have been about 0.5 micron, which equals the standard deviation. This error becomes significant for spacings below 4 microns. Others [4,8] have ignored coarse Si (flake in the partially modified sections) in their analysis. Figure 3 shows a completely modified structure. The fiber spacings were calculated as before.

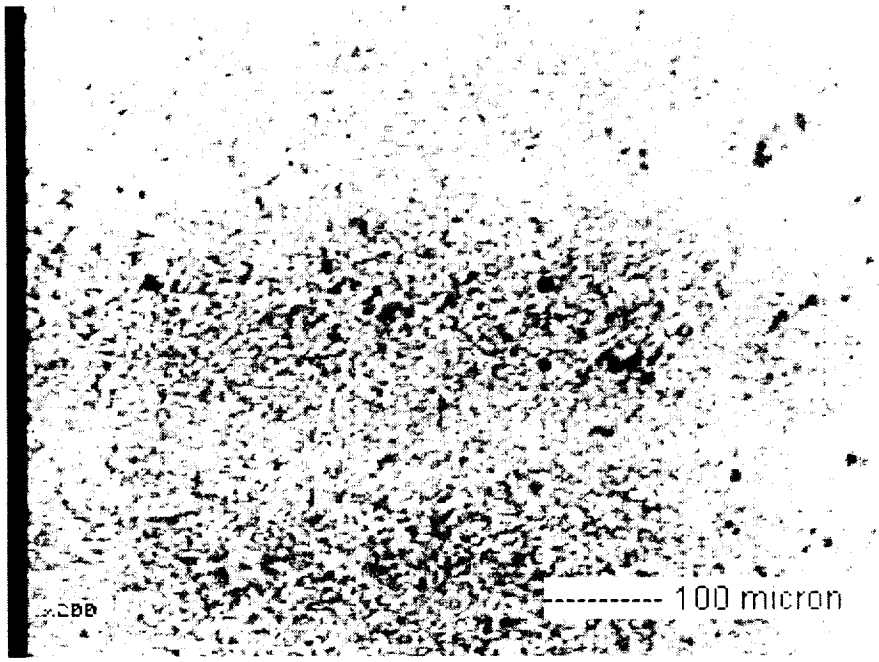

Figure 3. Transverse section cut 9 cm from bottom of the ingot. Translation rate = 32 mm/hr. Completely modified Al-Si. Magnification 200X.

We found only one instance [8] where the standard deviation was used to characterize Al-Si microstructure. Calculation of standard deviations and other readily available statistical measures has been emphasized by ASM. Comparing only the average spacings for ingots solidified under different conditions would result in serious error because the spacings in Al-Si show considerable scatter. Thus, in the present figures the standard deviation is given by the error bars on the average values. Figures 4, 5 and 6 show the variation of average eutectic spacing with translation rate in the three sections. Figure 4 shows negligible trend with translation rate, except for an increase in the standard deviation at rates greater than 40mm/hr. Figure 5 shows a small decrease of average spacing with no effect on the standard deviation. Figure 6 shows a decrease in standard deviation between 20 and 60 mm/hr.

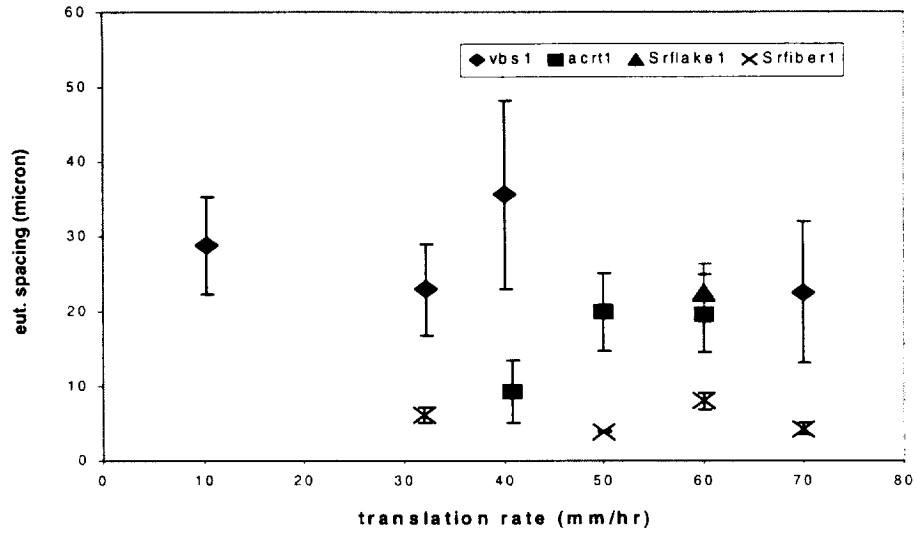

Figure 4. Eutectic spacing vs translation rate for a section about 8 cm from the start of growth. Vbs1 was solidified without ACRT, Acrt1 with ACRT. Srflake1 denotes flake spacing. Srfiber1 refers to fiber spacing.

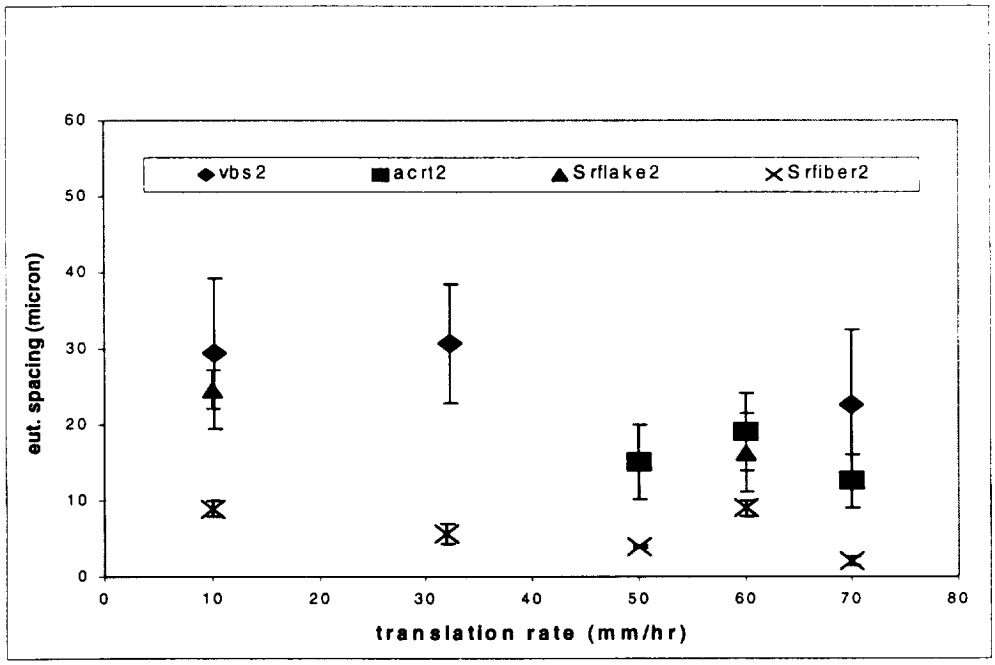

Figure 5. Eutectic spacing versus translation rate for a section about 5 cm from the start of growth. Vbs2 is without ACRT. Acrt2 is with ACRT. Srflake2 denotes silicon flake spacing. Srfiber2 refers to silicon fiber spacing.

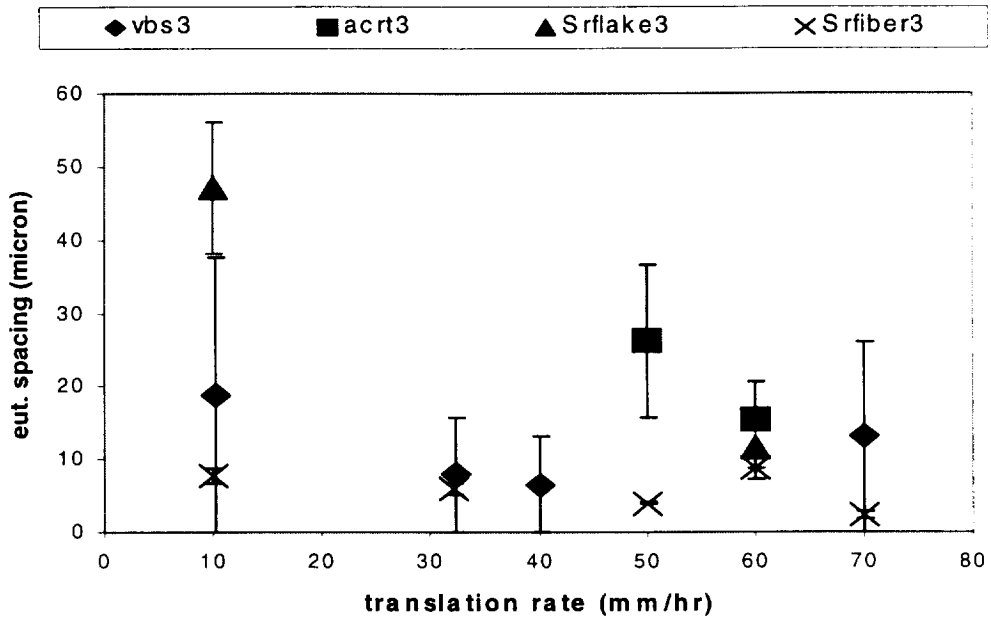

Figure 6. Eutectic spacing versus translation rate for a section about 5 cm from the start of growth. Vbs3 is without ACRT, Acrt3 with ACRT. Srflake3 denote silicon flake spacing, Srfiber3 silicon fiber spacing.

Let us see if we can draw conclusions about the influence of ACRT. Figure 4 indicates that up to 50mm/hr ACRT decreased the spacing in section 1 but has no effect on the standard deviation. Figure 5 indicates that ACRT decreased both the average and the standard deviation. Figure 6 shows that ACRT increased the average spacing and decreased the standard deviation in the bottom portion of the ingot. These trends may reflect the influence of ACRT on axial variations in the alloy composition, particularly the habit modifier Sr. Figure 5 indicates that in section 2 doping with Sr reduces the average spacing and the standard deviation. The effect is more pronounced in fiber-like Si whereas flake-type Si seems to follow the same trend as without ACRT. In section 3, though Sr doping reduces the average spacing and the standard deviation, the scatter without ACRT is so large that it is risky to draw any conclusion.

Figures 7, 8, and 9 show the variation of aluminum dendritic spacing and radius with solidification conditions. Some of the samples grown without ACRT were etched with dilute HCl, and it is quite possible that dendritic structures were dissolved. There were no dendrites in Sr-doped samples.

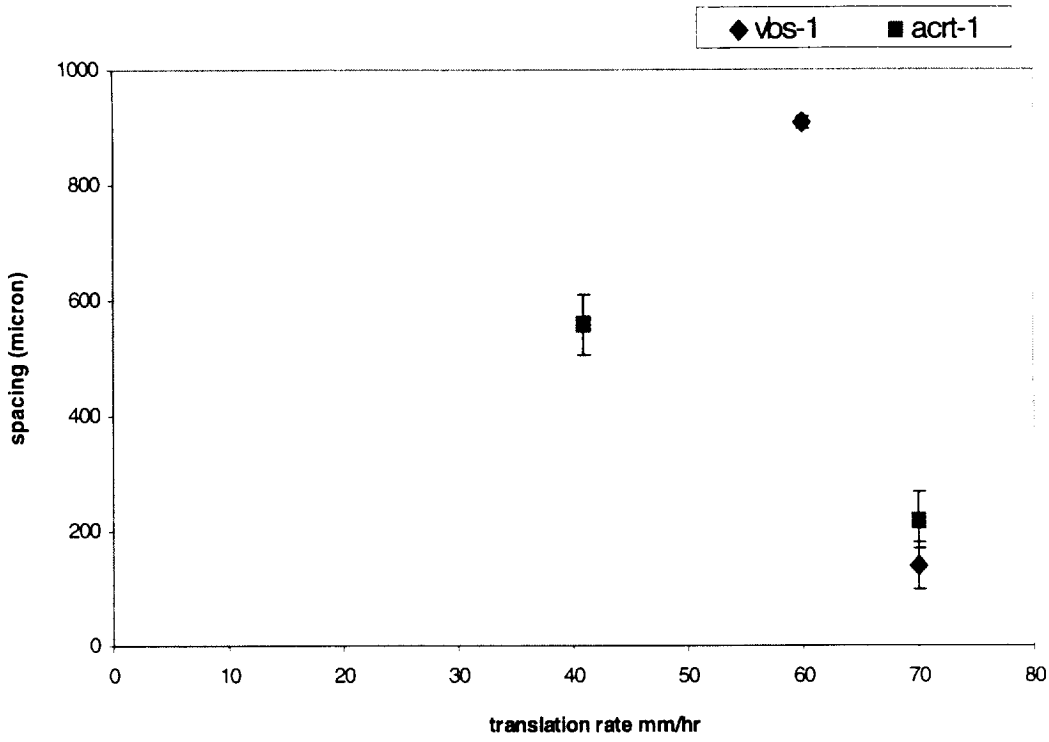

Figure 7. Primary aluminum dendrite spacing versus translation rate for a section about 8 cm from the start of growth. Vbs1 denotes no ACRT and Acrt1 with ACRT.

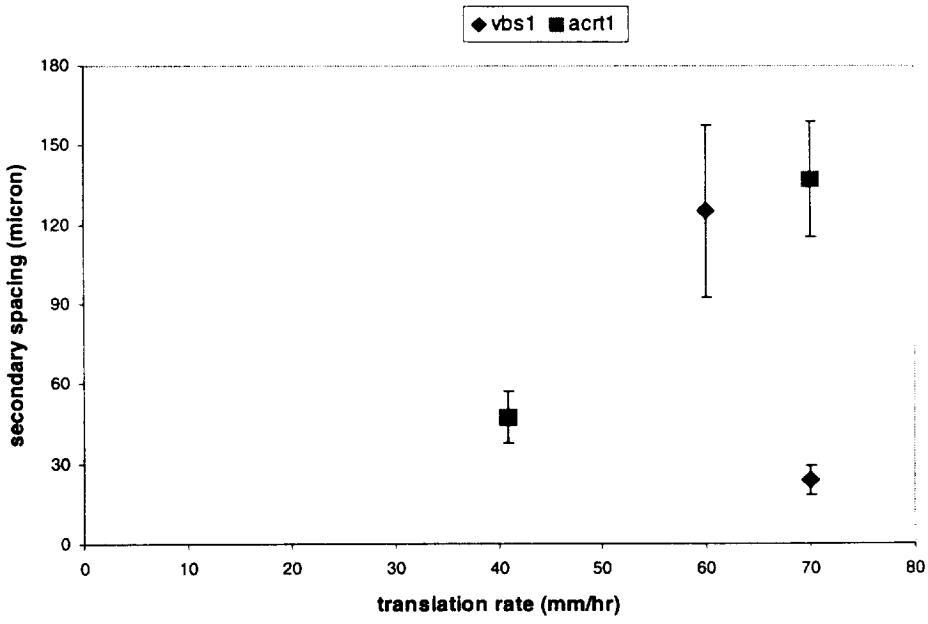

Figure 8. Secondary aluminum dendrite spacing versus translation rate for a section about 8 cm from the start of growth. Vbs1 denotes no ACRT, while Acrt1 indicates solidification with ACRT.

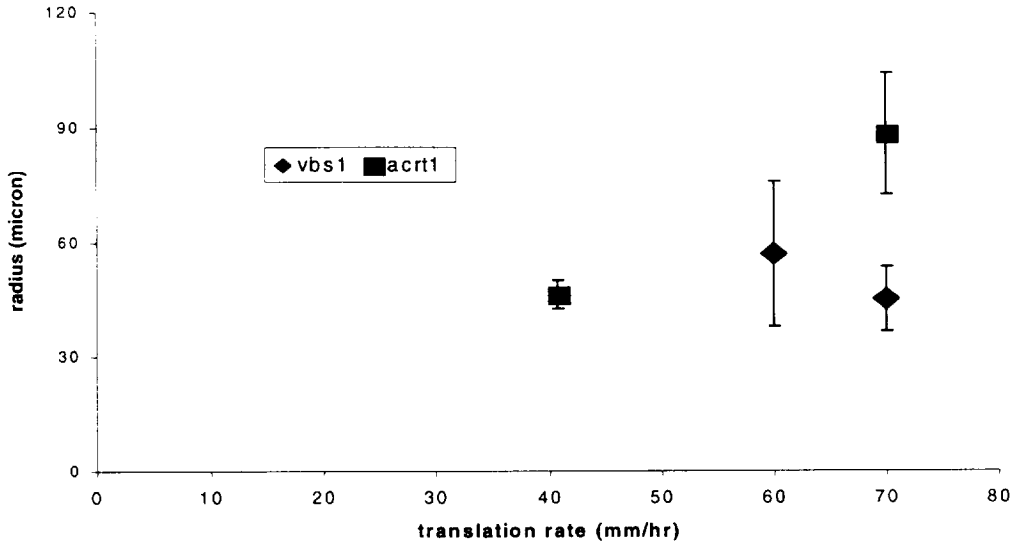

Figure 9. Secondary dendrite spacing versus translation rate for sections about 8 cm from the start of growth. Vbs1 without ACRT, Acrt1 with ACRT.

Comparison with literature

Figure 10 shows the present spacings obtained with unmodified alloys compared to the results of Hogan and Song (110K/cm) [8], Elliot and Glenister (8K/cm) [5,14], and Toloui and Helawell (150K/cm) [4,14]. The Sr flake data at translation rates of 10 and 60 mm/hr refer to partially modified structures. The spacings obtained by us are 2 to 3 times those reported in the literature. The closest is Sr flake spacing obtained at 60 mm/hr. The trendlines shown are for $\lambda^{2.19}V = 990$ (Hogan and Song) [8], and $\lambda^{3}V = 18576$ (Elliot and Glenister) [5,14] where λ is in μm and V in μm/s. This indicates that no definite conclusion can be drawn for unmodified eutectics and that the extremum condition [11] is not obeyed, as suggested by Elliot [5,14] and Hogan [8]. We conclude that in absence of Sr and in the range of translation rates studied, there is no apparent influence of translation rate on eutectic spacing. In partially modified structures, the spacing decreased with increasing translation rate in the top and middle portions of the ingot. Figure 11 shows modified Al-Si spacing compared to the values obtained in the literature. Other than the fiber spacings obtained in partially modified samples, our spacings are near those of Hogan and Song (110K/cm) [8], Elliot and Glenister (8K/cm) [5,14] and Atasoy (120K/cm) [6,14].

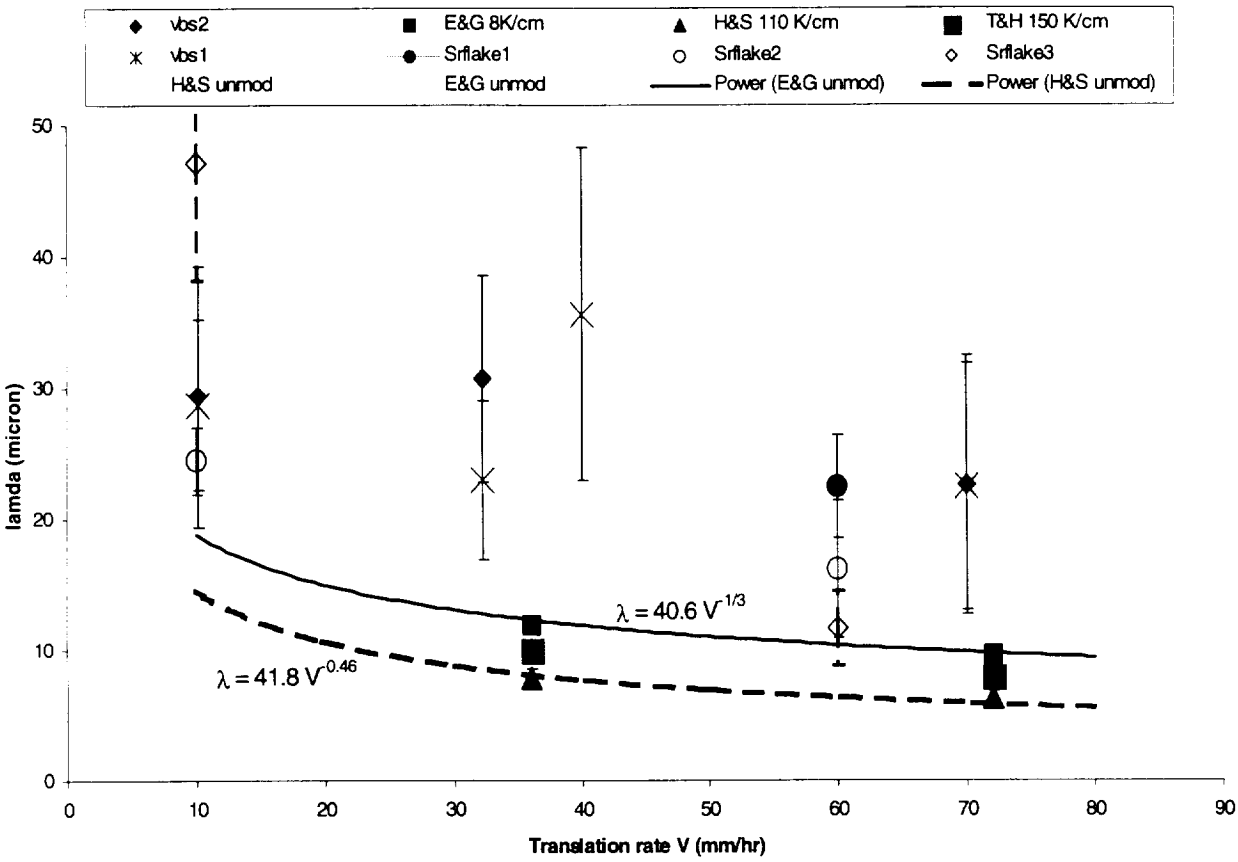

Figure 10. Current results compared to those reported in the literature for unmodified Al-Si. The dashed curve represents the relation $\lambda^{2.19} V = 990$ (Hogan and Song) and the solid curve, $\lambda^3 V = 18576$ (Elliot and Glenister), with λ in μm and V in μm/s.

Sens *et al.* [13,14] reported convection enriches the solid in Al, primarily by formation of more Al dendrites. This effect increased with increasing Sr doping. In the range of translation rates studied here we did not observe any dendrites when the eutectic was doped with Sr. We observed dendrites only at translation rates exceeding 40 mm/hr, both with and without ACRT. And these dendrites were seen only in the top portions of the ingots. The trendlines seen in Figure 11 are for $\lambda^{2.24}V = 422$ (Hogan and Song) [8], $\lambda^2 V = 157.5$ (Elliot and Glenister) [5,14], and $\lambda^3 V = 310$ (Atasoy) [6,14], where λ is in μm and V in μm/s. Thus we see that completely modified structures lie between the region suggested by Hogan and Song [8] and Atasoy [6,14]. This does not agree with Elliot and Glenister's [5,8] observation that the λ-V relationship fluctuates between $\lambda^2 V$ and $\lambda^3 V$ for modified eutectics. However the freezing rates studied by them varied between 36 and 400 mm/hr and many readings were not taken in the 10-70 mm/hr range. For partially modified eutectics, there is a need for more experiments to determine a λ-V relationship.

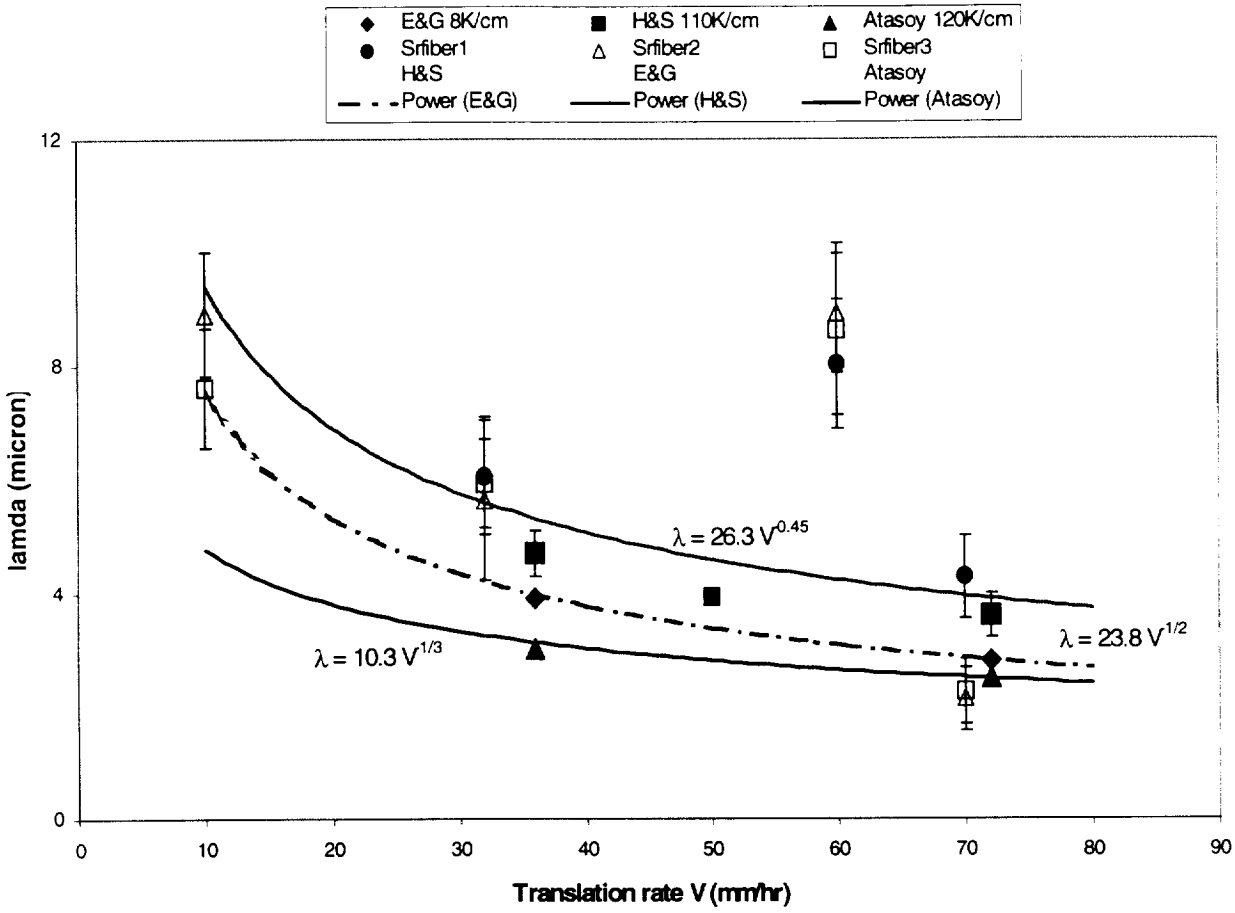

Figure 11. Present results compared to those reported in the literature for completely modified Al-Si. The topmost curve represents the relation $\lambda^{2.24}V = 422$ (Hogan and Song), the middle curve $\lambda^2 V = 157.5$ (Elliot and Glenister), and the bottom curve $\lambda^3 V = 310$ (Atasoy) where λ is in μm and V in μm/s.

References

1. P. Borgeaud, F. Dabel and M. Drouzy, "Structure and Modifications of Al-Si alloys close to the Eutectic," *AFS Cast Metals Research Journal*, (September 1968), 151-158.
2. H.A.H. Steen and A. Helawell, "Structure and Properties of aluminum-silicon eutectic alloys," *Acta Metall.*, **20** (1972) 363-370.
3. D.C. Jenkinson and L.M. Hogan, "The Modification of aluminum-silicon alloys with strontium," *J. Crystal Growth*, **28** (1975) 171-187.
4. B. Toloui and A. Helawell, "Phase Separation and Undercooling in Al-Si eutectic alloy - The influence of freezing rate and temperature gradient," *Acta Metall.*, **24** (1976) 565-573.
5. R. Elliot and S.M.D. Glenister, "The Growth Temperature and Interflake Spacing in aluminum silicon eutectic alloys," *Acta Metall.*, **28** (1980) 1489-1494.
6. O.A. Atasoy, F. Yilmaz and R. Elliot, "Growth structures in Aluminum-Silicon alloys" *J. Crystal Growth*, **66** (1984) 137-146.
7. L. Clapham and R.W. Smith, "The mechanism of the partial modification of Al-Si eutectic alloys," *J. Crystal Growth*, **79** (1986) 866-873.
8. L.M. Hogan and H. Song, "Interparticle spacings and undercoolings in Al-Si eutectic microstructures," *Metall. Trans A*, **18A** (1987) 707-713.
9. L. Clapham and R.W. Smith, "Segregation Behavior of Sr in modified and unmodified Al-Si alloys," *J. Crystal Growth*, **92** (1988) 263-270.
10. L. Clapham and R.W. Smith, "Partial Modification in unidirectionally solidified Al-Si eutectic alloys," *Acta Metall.*, **37** (1989) 303-311.
11. K.A. Jackson and J.D. Hunt, "Lamellar and rod eutectic growth," *Trans. TMS-AIME*, **236** (1966) 1129-1142.
12. D.J. Fisher and W. Kurz, "A theory of branching limited growth of irregular eutectics," *Acta Met.*, **28** (1980) 777-794.
13. B. Drevet, D. Camel and J.J. Favier, "Solute boundary layer and convection in solidification of eutectic alloy," Proceedings VIIth European Symposium on Materials and Fluid Sciences in Microgravity, Oxford, UK, (September 1989), 101-108.
14. H. Sens, N. Eustathopoulos, D. Camel and J.J. Favier, "Solidification of binary and Sr modified Al-Si eutectic alloys: theoretical analysis of solute fields," *Acta metall. mater.*, **40** (1992) 1783-1789.
15. P. Magnin, J.T. Mason and R. Trivedi, "Growth of irregular eutectics and the Al-Si system," *Acta metall. mater*, **39** (1991) 469-480.
16. R. Trivedi and W. Kurz, "Solidification microstructures: a conceptual approach," *Acta metall. mater.*, **42** (1994) 15-23.
17. J. Zhou, "Accelerated Crucible Rotation Technique and Current Interface Demarcation during Directional Solidification of Te-Doped InSb," M.S. Thesis, Clarkson University, Potsdam, NY, (1992).

MODELING OF OSCILLATORY EUTECTIC SOLIDIFICATION

Dmitri Popov

Abstract

Three related approaches were used to model an eutectic solidification with an oscillatory freezing rate. A sharp interface model was used to find the composition oscillations at the freezing interface as a response to imposed freezing rate oscillations, both analytically and numerically. The changes in supersaturation and undercooling were used to predict microstructure transformations due to nucleation. A numerical solution was also obtained for one phase is leading and for the temperature oscillating at some distance from the interface.

Another model was based on the principle of minimum entropy production for stationary periodic systems. We calculated the steady state and stationary periodic entropy production for eutectic system. Expressions were found for spacing λ for growth at a constant freezing rate, oscillatory growth, and with a modulated freezing interface.

The third approach used the phase-field method [1]. This method produced real-time patterns of phenomena involved in microstructure variation, including nucleation, lamella termination, oscillatory instability, broken lamellar growth, and banding. The understanding of the mechanisms responsible for the change of the microstructure allowed us to explain the evolution of the microstructure in an oscillating temperature field. The method can not only describe the propagation of lamellar faults, but also is able to handle catastrophic changes in microstructure, such as nucleation of a new phase or lamella elimination.

All three models predict a decrease in λ when the freezing rate oscillates.

Sharp-interface model

Analytically, we found the solution for the oscillatory part of the composition in the melt:

$$\frac{\partial^2 c^{(1)}}{\partial x^2}+\frac{\partial^2 c^{(1)}}{\partial z^2}+\frac{V_0}{D}\frac{\partial c^{(1)}}{\partial z}+\frac{V_0}{D}\sin(\omega t)\frac{\partial c^{(0)}}{\partial z}=\frac{1}{D}\frac{\partial c^{(1)}}{\partial t} \qquad (t\to\infty) \tag{1}$$

where $c^{(1)}$ is the first order expansion of the composition in the melt by a small parameter, the amplitude of the freezing rate oscillations, $c^{(0)}$ is the steady state solution [3], ω is the oscillation frequency, V_0 is the freezing rate, D is the diffusion coefficient, x and z are the spatial variables, and t is time. For small λ, the oscillating part of the composition field can be described by an amplitude coinciding with the deviation of the composition from the eutectic composition at steady state, and by a phase lag φ between freezing rate and composition oscillations:

$$c^{(1)}\big|_{z=0}=\delta c\big|_{z=0}\sin(\omega t-\varphi) \tag{2}$$

where $\delta c\big|_{z=0}=c^{(0)}\big|_{z=0}-c_E$ and c_E is the eutectic composition (see Figure 1).

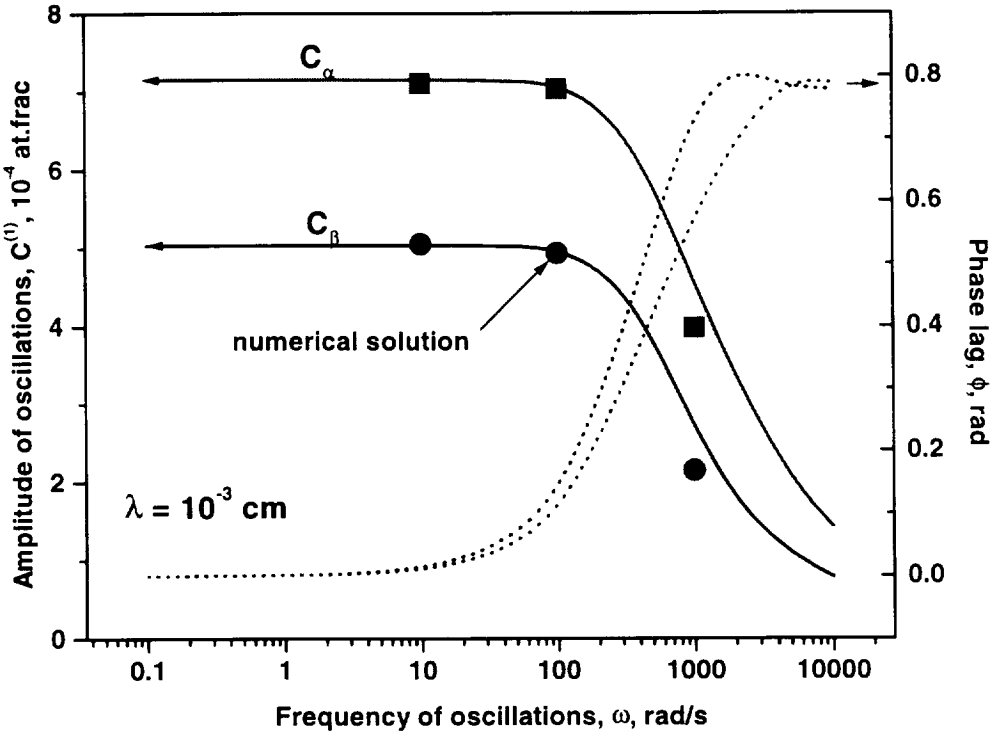

Figure 1. Amplitude and phase lag of the oscillating composition at a freezing interface caused by freezing rate oscillations. The curves are for $\lambda=10^{-3}$ cm, difference between the terminal solid compositions c_β-c_α =0.696, segregation coefficients k_α=0.392, k_β =1.334, diffusion coefficient $D=10^{-5}$ cm^2/s, and average freezing rate $V=10^{-4}$ cm/s. The result was obtained using the sharp interface model.

■ , ● - **Numerical results for the composition of α and β phases, respectively.**

_____ - **Analytical solution for the amplitude of oscillations in local composition field at the interface.**

- - - - - - - **Analytical solution for the phase lag of composition oscillations from freezing rate oscillations.**

The phase lag depends on the interplay between the oscillation frequency and the inverse diffusion time in the lateral direction, and plays an important role in increasing the undercooling at the interface. The phase lag can be as large as $\pi/4$, depending on the lamellar spacing, oscillation frequency, freezing rate, and melt diffusion coefficient. The oscillations originating from an off-eutectic diffusion layer can be significant, especially for small λ and large ω.

The effect of a lead of one phase over the other is to cause the average interface composition to be off-eutectic. For a system where volume fraction adjustment is permitted, that would set a new volume fraction to satisfy the interfacial material balance. In the model we used, volume fraction adjustment through the propagation of lamellar faults is prohibited, and a lead causes an increase in the amplitude of the compositional oscillations at the interface of the leading phase. This leads to an increase of the excess average undercooling of the leading phase. The larger the lead distance, the larger the difference between the amplitudes of the freezing rate oscillations of

the leading and trailing phases. As a result, the excess undercooling is larger and may result in morphological changes.

A simple nucleation model supported the viewpoint that nucleation of new lamellae shifts the average interface composition away from eutectic. We were able to distinguish several possible scenarios when the freezing rate oscillates:

1. Neither α nor β can nucleate and growth remains within coupled zone.
   a. For roughly symmetric (volume fraction $\zeta \approx 0.5$) eutectics with equal liquidus slopes at the eutectic temperature $|m_\alpha| \approx |m_\beta|$, there is no change in microstructure.
   b. For asymmetric eutectics, the average composition of the interface becomes off-eutectic. The general trend is for λ to increase, especially for small ζ [4,5].
2. Only one phase (e.g., β) can nucleate and growth remains in the asymmetric coupled zone.
   a. If α trails, the microstructure does not change.
   b. If α leads, nucleation of β leads to an increase in the thickness of the diffusion layer. The resulting value of λ depends on the supersaturation necessary for nucleation.
3. Both α and β can nucleate so that growth moves outside of the coupled zone. The average interfacial melt composition remains at the eutectic, with smaller amplitude composition oscillations than above. The eutectic spacing λ is smaller than at constant freezing rate.

Although the sharp-interface model is not able to set the conditions for triggering catastrophic morphological changes as a part of its solution, it is able to predict what changes to expect when those conditions are specified.

Entropy production model

The steady-state eutectic spacing λ_{SS}, neglecting the effect of the interface non-planarity on the melt composition near the interface, was determined using the principle of minimum entropy production to be:

$$\lambda_{SS} = \sqrt{\frac{2D\left\{\Delta S_\alpha \Gamma_\alpha \sin(\theta_\alpha) + \Delta S_\beta \Gamma_\beta \sin(\theta_\beta)\right\}}{V c_0 P(\zeta)\left\{\frac{RT_E c_0}{v_m c_E (1-c_E)} + \left(-\Delta S_\alpha m_\alpha + \Delta S_\beta m_\beta\right)\right\}}} \tag{3}$$

where ΔS is the entropy increase upon melting, Γ is the Gibbs-Thomson coefficient, θ is the angle at the tri-junction, v_m is the molar volume, and T_E is the eutectic temperature. The other variables come from Jackson-Hunt formulation [3]. For a symmetric eutectic, the two terms in the denominator of (3) are approximately equal and the Jackson-Hunt solution based on the principle of minimum undercooling can be recovered. We have also shown that the effect of a finite lead distance is to make λ larger than for a planar interface when the volume fractions of the two phases are significantly different.

The average curvature along the α/liquid interface, averaged over one period of oscillation, is:

$$\overline{\kappa} = \sin(\theta_\alpha) \tag{4}$$

which is independent of the interface depression that changes during an oscillation. This result suggests that, in spite of the fact that the interface shape oscillates, the average interface curvature is time independent. In the solution of the interface composition in the form of

equation (2), a time-dependent part could be separated from a spatially dependent part. The numerator inside the square root in equation (3) is time-independent, and, therefore, does not depend on the freezing rate oscillation amplitude ε or phase lag φ. The denominator is proportional to $1+\frac{\varepsilon^2}{2}\cos(\varphi)$. The new stationary periodic solution for λ obtained using the principle of minimum entropy production is:

$$\lambda = \lambda_{ss}\frac{\sqrt{2}}{\sqrt{2+\varepsilon^2\cos(\varphi)}} \tag{5}$$

where λ_{SS} is the steady-state spacing given by equation (3). The decrease in λ due to an oscillating freezing rate with dimensionless amplitude ε is shown in Figure 2. The two curves are for different phase lags between freezing rate and compositional oscillations. The value of λ is decreased only by 13-18% for a 100% freezing rate oscillation (ε = 1). (Backmelting (ε>1) is not considered here.)

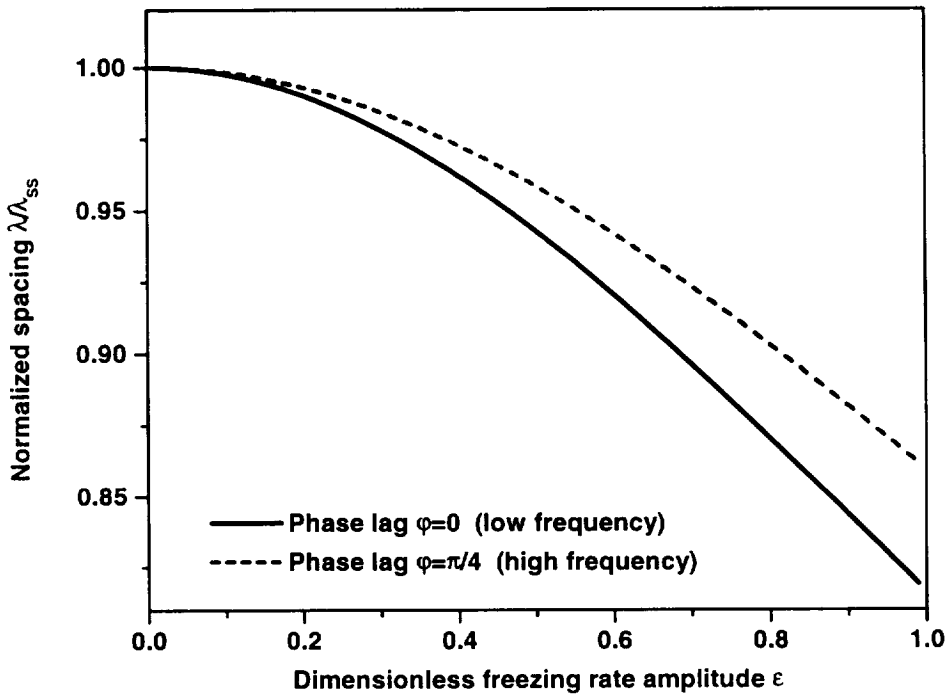

Figure 2. The decrease in λ due to freezing rate oscillations of dimensionless amplitude ε. Obtained using the principle of minimum entropy production.

We also examined the situation wherein a eutectic structure can grow with a modulated freezing interface due to interface instability. When the freezing interface is perturbed by current pulses as in the section of this report by Ms. Li [6], the interface may become unstable and modulated over a length scale larger than λ. For solidification from a eutectic melt, the interfacial material balance requires that at the center of the protruding part of the interface the average composition changes by c_K, whereas at the center of the depressed part of the interface

the average composition changes by - c_K. In such a case, interface modulation should cause a reduction in λ in some locations, while in others λ would be increased.

Phase-field model

In our phase-field calculations we used equal surface energies $\sigma = 6*10^{-5}$ J/cm^2 for all interfaces, with an interface width $\delta = 5*10^{-5}$ cm. A decrease in δ would have required an increase in the number of computational points, and, therefore, in CPU time. With $\delta = 5*10^{-5}$ cm it was possible to model numerically the physical domain $2*10^{-3}$ x $2*10^{-3}$ cm with 301 x 241 computational points in the lateral and growth directions, respectively. The relaxation parameter τ was chosen to be $\tau = 10^{-5}$ J.s/cm^3, to give a value for the linear kinetic coefficient β of about 30 cm/K.s. This value is several times lower than that possessed by metals, and, therefore, required more undercooling for the same growth rate. The time step was chosen $2*10^{-8}$ s, the Cray CPU time was estimated to be approximately $2*10^{-3}$ s per time step, or approximately 30 hr of calculating per 1 s of solidification.

Mechanisms responsible for changes in microstructure

Figure 3 shows that nucleation is followed by a rapid increase in the interface advancement rate. Nucleation increases interface undercooling by moving the average interfacial composition away from the eutectic. As the volume fractions of the two solids adjust, the system relaxes toward a new steady state with a new spacing λ. On the other hand, a drastic increase of the freezing rate does not follow termination of a lamella since the volume fraction changes gradually with the propagation of lamellar faults. Therefore, the average interface composition remains close to the eutectic and there is insignificant change in total undercooling.

Figure 4 shows a phase-field simulation for an increase in cooling rate by a factor of 6. It is concluded that the following are important for a decrease in λ:

(a) shape instability with formation of a deep groove;
(b) nucleation preceded by increased supersaturation in the deep groove. Nucleation destabilizes the interface;
(c) volume fraction adjustment that stabilizes the freezing interface.

The following process are important for an increase in λ:

(a) interface instability due to fluctuations of temperature and composition;
(b) volume fraction adjustment provided by the interface instability due to local change in growth direction;
(c) lamellar elimination as a mechanism stabilizing the interface.

Volume fraction adjustment stabilizes the interface when the growth rate is increased and destabilizes it when the growth rate is decreased.

At higher growth rates, oscillatory instability follows nucleation. This instability appears as an interplay between slow lateral diffusion and fast interface kinetics. At even higher growth rates, diffusion alone is not able to redistribute the composition in order to provide cooperative growth. The inevitable perturbations in temperature and composition fields break down the regular structure into irregular patterns. Banding takes place at even higher freezing rates, when the diffusion is not effective at all. A stable microstructure cannot be selected due to the absence of a mechanism to redistribute the rejected component along the freezing interface.

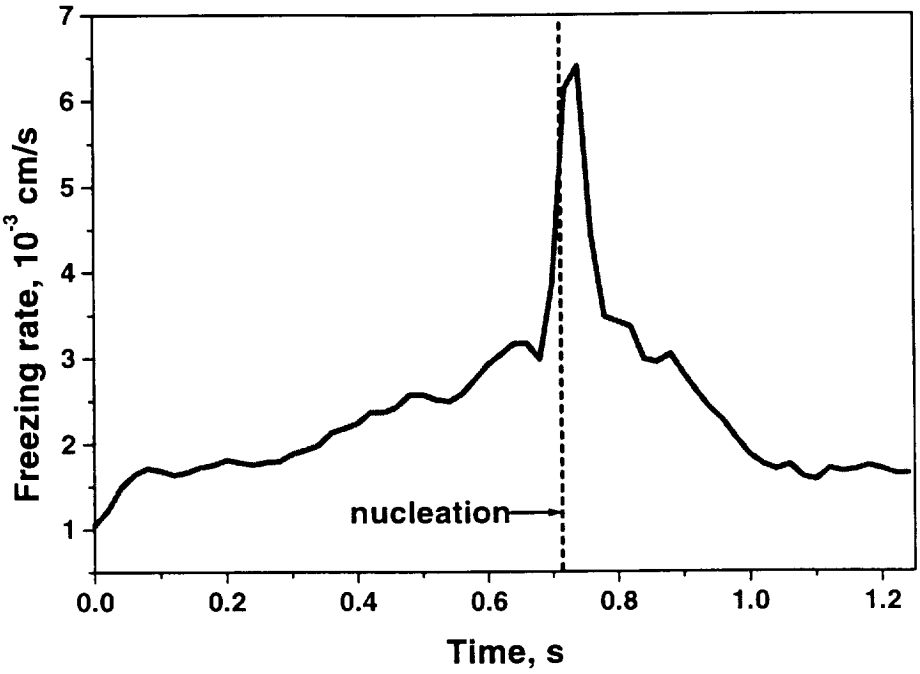

Figure 3. Sudden increase of the interface advancement rate caused by nucleation of a new phase. After nucleation, the interface advancement rate relaxes back to the value controlled by the rate of cooling. This result was obtained using the phase-field model.

Effect of temperature oscillations on eutectic microstructure

From our numerical results we conclude that the volume fraction adjustment mechanism for lamellar termination is not as significant as backmelting for large λ. A typical evolution is shown in Figure 5 for $\lambda = 8*10^{-4}$ cm. There are three ranges of oscillation amplitude that can change the microstructure when the freezing rate oscillates:

(a) low amplitude: no change in microstructure while the interface shape and volume fraction oscillate;
(b) intermediate amplitude: nucleation takes place. Either no backmelting occurs or, if it does, it does not restore the initial microstructure. As a result, the microstructure becomes finer;
(c) high amplitude: nucleation, backmelting, possible restoration of the initial morphology, or interface instability. Results in irregular growth or banding.

There are also three ranges of oscillation frequency that influence the eutectic microstructure:

(a) high frequency: there is no influence of an oscillating temperature field since, due to finite interface kinetics, the freezing interface is not able to respond. Growth proceeds at or close to steady state;
(b) intermediate frequency: the interface shape and volume fraction oscillate. For low amplitude oscillations, no changes are expected. For high amplitudes, an irregular morphology can follow nucleation and backmelting.
(c) low frequencies: depending on amplitude, the microstructure either becomes finer or backmelting results in the restoration of the initial microstructure.

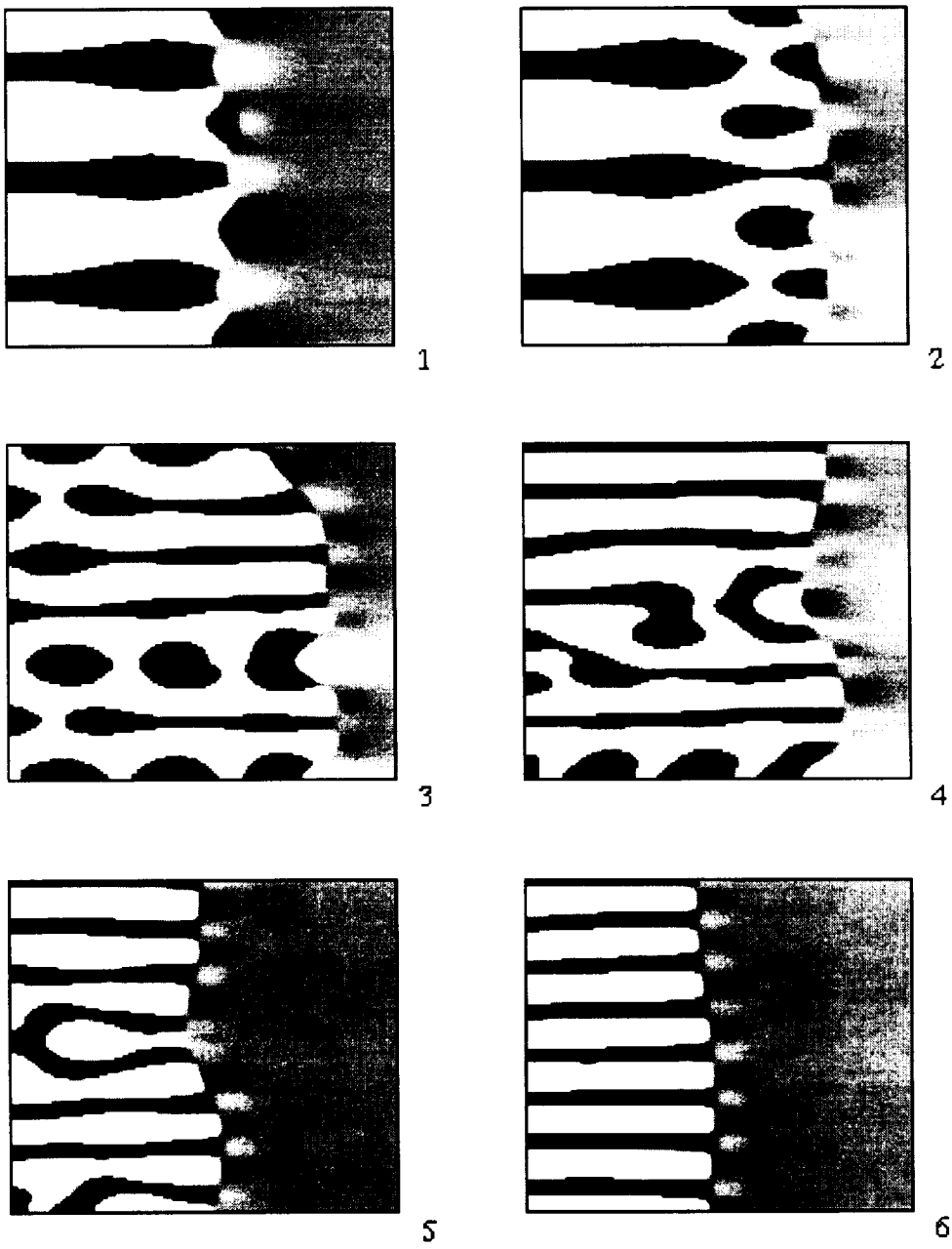

Figure 4. Evolution of a eutectic structure when the cooling rate is increased by a factor of 6. Initial $\lambda = 6.67*10^{-4}$ cm, final $\lambda = 2.67*10^{-4}$ cm. Black lamellae do not simultaneously nucleate at the centers of all white lamellae. Broken lamellae appear at the center of the freezing interface where the white phase is not wide enough to provide the supersaturation required for nucleation of the black phase. A new phase nucleates in the deep groove, and is then pinched off. Finally, a regular microstructure is selected and the freezing interface again becomes stable. Note the variation of composition in the melt, shown by different shades of gray.

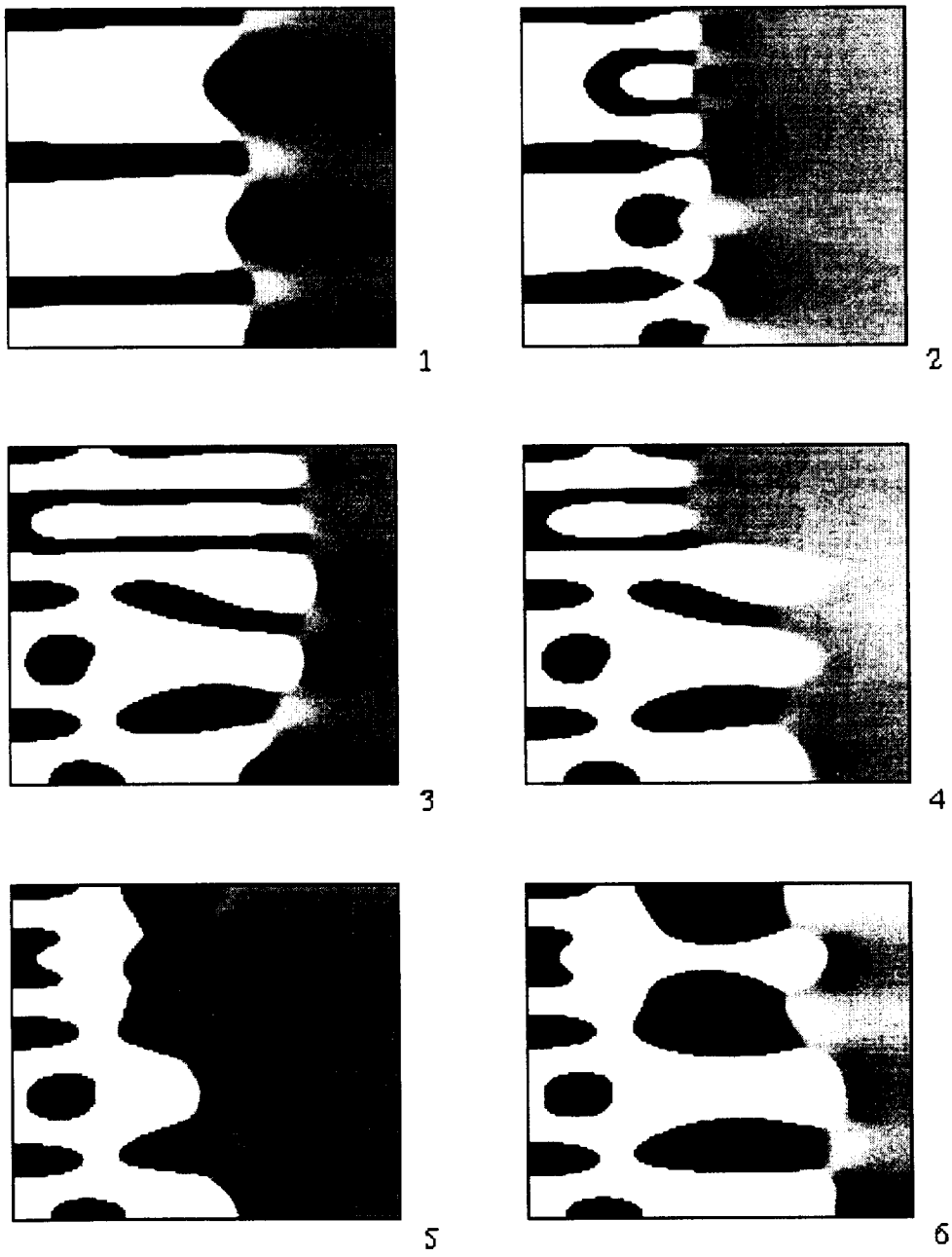

Figure 5. Evolution of a eutectic structure when the freezing rate oscillates. The amplitude of temperature oscillations is 10 K and the frequency is 2.5 Hz. Initially $\lambda = 8*10^{-4}$ cm. Nucleation of new phase occurs in the deep groove, followed by backmelting and restoration of the initial spacing λ.

Microstructure evolution is different for small and large eutectic spacings:

(a) high λ: nucleation readily takes place, and the volume fraction adjustment is stabilizing. For high oscillation amplitude, backmelting can restore the initial microstructure. Nevertheless, the interface shape and the composition field oscillate in time. The lower is the frequency of oscillation, the more dramatic are the changes in microstructure.

(b) Low λ: the destabilizing volume fraction adjustment becomes important. An oscillating diffusion layer is observed. Interface instability may lead to adjustment of volume fractions in the middle of the computational domain. The rates of phase nucleation and phase elimination are close, and both phenomena can occur.

Time scales for phase nucleation and phase termination

The time scales were estimated from order-of-magnitude analysis. The time scale for nucleation due to catastrophic shape instability was obtained from the assumptions that the growth rate increases at a constant rate, and that the volume fraction does not change until nucleation occurs. We used the result given by equation (2) and assumed that it is also valid for constant acceleration of the freezing interface, to obtain:

$$\tau_N = \frac{\Delta c^{NUCL} D}{V_t' c_0 \lambda \zeta P(\zeta)} \tag{6}$$

where Δc^{NUCL} is the excess supersaturation necessary for nucleation to occur, i.e. c^{NUCL}-c_{SS} (steady state corresponding to initial freezing rate). The higher is the supersaturation threshold for nucleation, the longer is the time needed to reach this threshold. A large diffusion coefficient D reduces the concentration of rejected component at the freezing interface, and so more time is needed until nucleation occurs. Finally, τ_N is inversely proportional to lamellar spacing λ and volume fraction ζ.

We assume that diffusion in the lateral direction controls the rate of volume fraction adjustment and phase termination. Again using equation (2) we find:

$$\tau_T = \frac{\lambda^{3/2}}{D}\sqrt{\frac{V_{SS} c_0 P(\zeta_{SS})\zeta_{SS}}{2c_t'}} \tag{7}$$

where τ_T is the time scale for phase termination, i.e. when the volume fraction ζ of α becomes zero. Here, c_t' is the rate of change of the average composition at the interface of one phase. From this order of magnitude analysis it follows that phase termination is more effective for small spacings. For large λ, oscillations would lead to nucleation during increasing freezing rate rather than to phase termination during decreasing freezing rate. As was shown by the numerical results, backmelting is more likely in this case.

The λ-dependence of the characteristic time for nucleation and phase termination is shown in Figure 6. The shaded area reflects the limitation of the phase-field model of eutectic solidification. Nevertheless, we were able to observe both nucleation and elimination of the phase through the motion of lamellar faults. It is not known what value of λ is the threshold value at which the system becomes unstable. The problem lies in the fact that the threshold for λ is not sharp, and the modeling was carried out close to computational limitations.

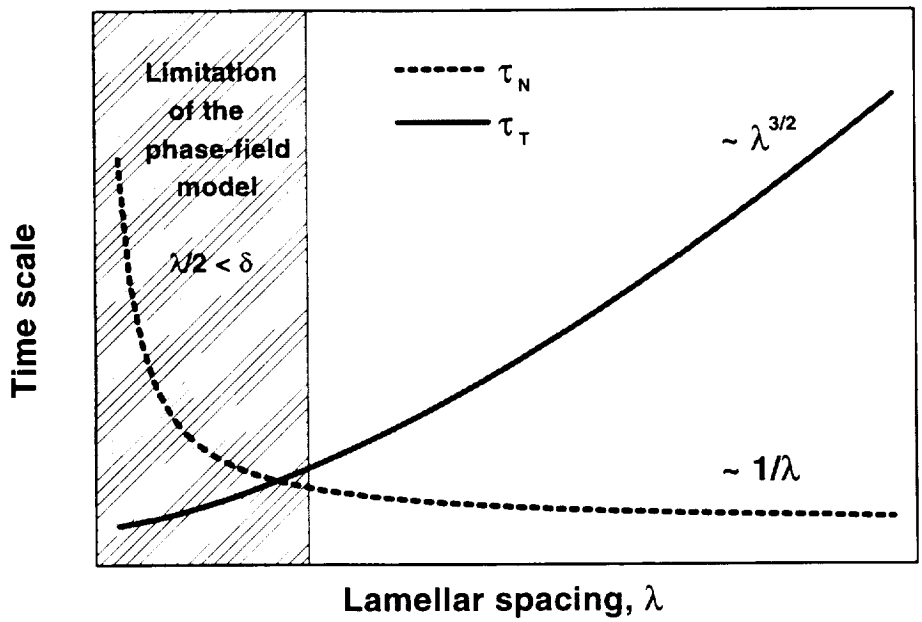

Figure 6. Time scales for lamellar nucleation τ_N (dashed curve) and lamellar termination τ_T (solid curve) as a function of lamellar spacing λ. The shaded area shows the range of λ where numerical solution using the phase-field model is impossible due to computational limitations.

References

1. G. Caginalp and W. Xie, "Phase-field and sharp-interface alloy models," *Phys. Rev. E,* 48 (1993) 1897-1909.
2. W. Shyy, in: "Computational Modeling for Fluid Flow and Interfacial Transport," Elsevier Science Publishers, Amsterdam (1994), pp. 353-463.
3. K.A. Jackson and J. Hunt, "Lamellar and Rod Eutectic Growth," *AIME Trans.* 236 (1966) 1129.
4. B. Drevet, D. Camel, and J.J. Favier, "Solute Boundary Layer and Convection in Solidification of Eutectic Alloy," Proc. VIIth European Symp. on Materials and Fluid Sciences in Microgravity, Oxford, UK, 10-15 September 1989, ESA SP-295 (January 1990), pp.101-108.
5. R. Caram, S. Chandrasekhar, and W.R. Wilcox, "Influence of Convection on Rod Spacing of Eutectics," *J. Crystal Growth,* 106 (1990) 294-302.
6. F. Li, L. Regel, and W. Wilcox, "The influence of Electric Current Pulses on the Microstructure of the MnBi/Bi Eutectic," to be submitted to *J. Crystal Growth.*